Silicate Glass Coating on Copper Nanoparticles and Its Further Application to a Transparent Corrosion Resistant Film for Magnesium Alloys

Shohei Shiomi

Department of Materials Science and Engineering,

Kyoto University

2014

Contents

Chapter 1

General Introduction

1.1 Introduction

Generally, a “metal” is a material that has good ductility, electrical and thermal conductivity, and characteristic shiny appearance. However, a metal is typically influenced by ambient environments, and as a result, corroded or oxidized. This weak point becomes much more pronounced when the size of metal gets smaller as the specific surface gets larger. On the other hand, an “oxide” generally has a good chemical and thermal stability. For example, Al develops a thin layer of oxides that protects the metal Al from further corrosion, which is called passivation. In terms of Al, the oxide layer is so thin and transparent that the shiny appearance or other features of metal Al are basically maintained. Like Al, some metals develop good passivation layers, but the others have thick oxide layers or cannot stop the further oxidation, which induces the loss of characteristic properties of metals. Cu is a representative example of a metal whose appearance remarkably changes by the oxidation in both dry and wet environments. In air, the black CuO layer formed by an oxidation covers the surface of metal Cu, and the original metallic surface gets lost with time. Cu is also damaged in solutions as the dissolution by an oxidation.[1-4]

The aim of this study is to stabilize metals by the oxide-coating. Especially, we focus the core-shell structure of $Cu@SiO_2$, namely SiO_2-coated Cu. Silica is an oxide that shows a remarkable chemical and thermal stability. It will also keep the color of core metals, since silica is a transparent material. We investigate the method of silica-coating and suggest the evaluation techniques for measurement of the stability of core metals in solutions. As the

application of synthesized Cu@SiO_2 particles, we also report the approaches to red color glaze for ceramics. Furthermore, the silica-coating of magnesium for the improvement of corrosion resistance is also reported.

In the following of this chapter, a brief overview about fabrications and features of metallic copper nanoparticles is described, and the sol-gel process is introduced, which is the general method for oxide-coating. Then, the description about glaze for ceramics or pottery is briefly described. At the end of this chapter, the outline of the present study will be formed.

1.2 Copper nanoparticles

Nanoparticles are used in various fields as magnetic recording materials,[5,6] biomaterials,[7,8] catalysts,[9,10] inks for printed electronics,[11-13] optical sensors,[14,15] pigments,[16,17] etc. The synthesis and characterization of nanoparticles is widely investigated in the world. Various synthesis methods of nanoparticles are suggested in both top-down and bottom-up approaches. In the top-down approach, particles are fabricated by mechanical crushing of the source materials using a milling process.[18-20] In the bottom-up approach, structures are built up by chemical processes.[21-23] The selection of the respective process depends on the chemical composition and the desired features specified for the nanoparticles. We have investigated the electroless deposition method for the fabrication of metallic nanoparticles such as Cu, Co, Ni.[24-26] In this method, metallic nanoparticles are formed by mixing two solutions containing a precursor of the metal and a reducing agent as shown in Figure 1.1. The nucleation and growth of the particles proceed in the simultaneous reactions of oxidation of the reducing agents and reduction of metallic ions, and nanoparticles are precipitated in the solution as long as the reducing agent works. However, once the reducing agent is

decomposed or exhausted, the reducing ability of the solution decreases, and the metallic nanoparticles are oxidized again.

Cu is a reddish metal with good thermal and electrical conductivity, and it has an advantage for its lower cost than the other noble metals. Moreover, nanoparticles of Cu show the characteristic dark red color like blood due to the surface plasmon resonance, and they are capable of wide variety of optical applications.[27-29] However, Cu nanoparticles are remarkably sensitive to the oxidation,[30] and the unique color or other features of metallic Cu nanoparticles are easily lost even at room temperature. For instance, when Cu nanoparticles or Cu pastes are commercially offered, some manufacturers give a moderate oxidation to the synthesized nanoparticles by an air bubbling for avoidance of a complaint about color change after breaking a seal. Therefore, the investigation for the stabilization technique of metallic Cu attracts a great deal of attention.

1.3 Sol-gel process

The sol-gel process is a method for fabricating oxides by chemical reactions in a solution at relatively low temperature. In this work, we focused silicate glass (silica, SiO_2) as a stable oxide-coating layer. Silicate glass is industrially produced by melting the ingredients over 1773 K. On the other hand, the glass fiber used for an optical fiber needs an enormously high transparency, and it is generally produced by a vapor phase reaction. However, these producing method need high temperatures or operations of complex equipment. The sol-gel process is relatively new method with a simple procedure compared with the melting method and the vapor phase reaction method.[31-33] In the sol-gel process, tetraethyl ortho silicate (TEOS) is one of the most famous precursors of silica. Figure 1.2 schematically shows the

reactions of TEOS in the sol-gel process. First, the hydrolysis reaction proceeds by a water with a catalyst of acids or bases. In order to make a uniform mixture of TEOS and water, these chemicals are generally reacted in the alcohol solution. Next, the condensation reaction proceeds by molecules of water dissociated from $Si(OH)_4$ with a generation of bridging oxygen. By the continuous progress of these hydrolysis and condensation reactions, through a stage of sol, silica gel is finally formed. Since this silica gel still contains water molecules and unreacted hydroxyl groups, an appropriate heat-treatment is necessary to obtain the tight silicate glass. As shown in Figure 1.3, the weight of silica fabricated by sol-gel process decreases in heat-treatment, which indicates that the remaining water molecules are vaporized and the unreacted hydroxyl groups are well-condensed by heat-treatment.

As the basic catalyst for the hydrolysis reaction of TEOS, ammonia (NH_3) is often chosen, but sodium hydroxide (NaOH) is rarely used. This is because NaOH has a low catalytic activity of condensation reaction in sol-gel process. Na is a network modifier of silica as shown in Figure 1.4, and thus it disturbs the homogeneous bridging of Si-O-Si.[34-36] As a result, non-uniform and small silica particles are obtained when NaOH catalyst is used as shown in Figure 1.5. Moreover, since the Na remains in a network of silica even after the heat-treatment, purity of fabricated glass is low. Therefore, NH_3 should be used as the basic catalyst for sol-gel reaction to synthesize the uniform and pure silica.

1.4 Glaze

A pottery or china is generally coated by a glassy layer to give it colors, decorations, strength or waterproofing property, and this coating layer of glass is called “glaze”. Various kinds of glazing techniques have been developed by many peoples in many places since

ancient times. Originally, glazes were obtained by firing a mixture of clay with wood ashes or straw ashes. In this process, glazes were colored by metallic components contained in the clays or ashes. But recently, in order to get desired colors or decorations, metal components are mixed in advance.[37,38]

Glazes are typically classified based on the firing temperature. From a historic point of view, the inception of oriental glaze is ash glaze or feldspathic glaze. These glazes need high temperature (more than 1473 K) for firing; in other words, the melting point of these glazes is high, since these glazes have a relatively high SiO_2 content. Glazes which need high firing-temperature like ash glazes or feldspathic glazes are called “high-temperature glaze”. On the other hand, “low-temperature glaze” which is melted less than 1473 K is sometimes desired. To lower the melting point of glazes, alkali metal elements or borate components are mixed with feldspars, and by crushing this mixture, water-insoluble glass frit is formed. The fritted glazes are often used for “overglaze” decoration. Overglaze is a coloring method for giving an already-glazed product a more colorful, decorative, and glassy look.[39]

Figure 1.6 shows the appearances of some glazes which contain the same amount of pigment, which strongly suggests that the color of glaze is dramatically influenced even by the glass matrix or firing atmosphere. Therefore, the scientific investigation of glaze is awfully complicated since it needs complex analysis of multicomponent systems and optimization based on artisanal techniques. However, the further academic investigation will certainly help the development of glazes and glass science, and thus, it is indispensable also for the growth in art and industry in this field.

1.5 Outline of this study

The outline of this study is explained in Figure 1.7. The following are detailed descriptions of each chapter.

In chapter 2, the synthesis method of silica-coated Cu nanoparticles via electroless deposition and sol-gel process is proposed. The most important concept in this coating process is preservation of core metals during the formation of coating layers. Therefore, the evaluation of the stability of core metals and the measurement of reaction rate is of great significance. We suggest the evaluation method of the stability of core metals in a solution using QCM measurements combined with electrochemical measurements. This evaluation offers valuable insight for the paradigms of the relationship between thermodynamics and kinetics.

In chapter 3, the application of silica-coated Cu nanoparticles for red color glaze is described. The silica-coated Cu nanoparticles are mixed with glass frit and heat-treated to check if they can be used as the pigment of red color glaze for overglaze decoration. We demonstrate that the silica shells efficiently protect the Cu-core from oxidation even during the heat-treatment for the fabrication of glaze.

In chapter 4, the silica-coating method is expanded to a coating of bulk materials as transparent corrosion resistant films. We try the dip coating of bulk Cu and Mg using trifunctional alkoxysilane with the expectation for the flexibility of coating layer and good adhesion property to the metal substrates.

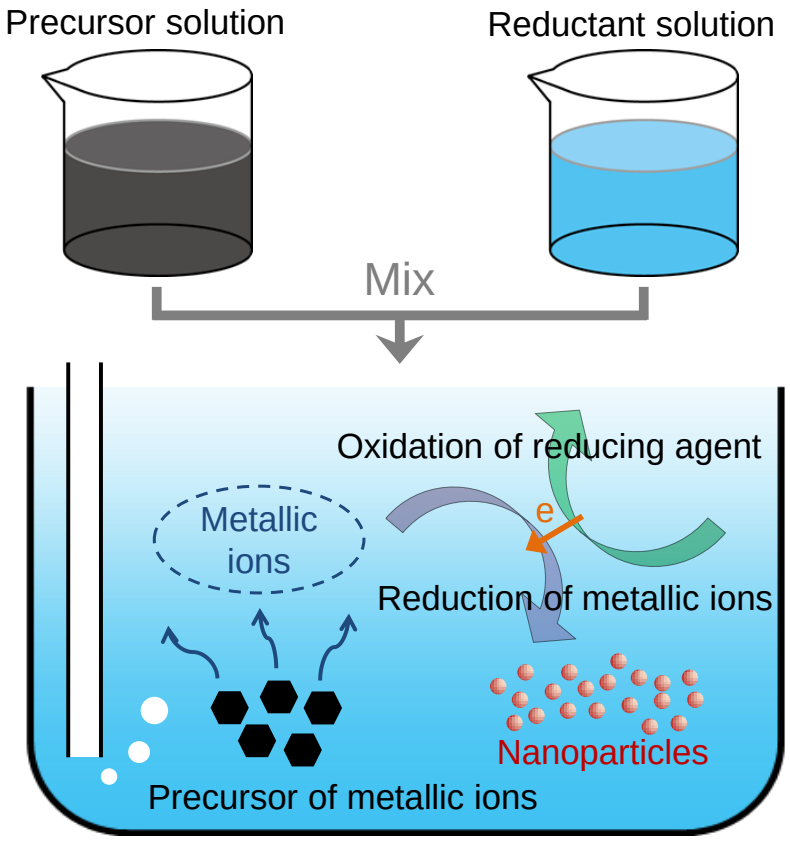

Figure 1.1 Schematic illustration of eletroless deposition for synthesis of nanoparticles.

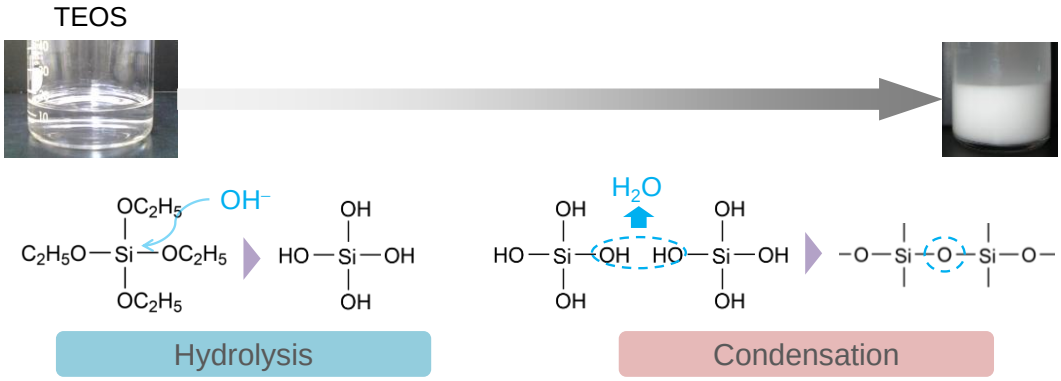

Figure 1.2 Photograph of silica fabricated from TEOS and simplified reaction formulae of hydrolysis and condensation of TEOS.

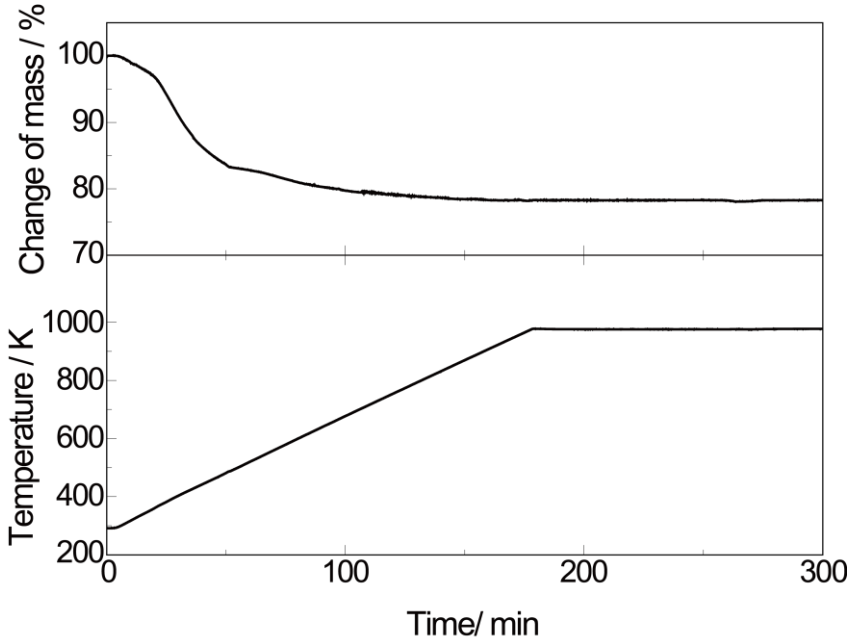

Figure 1.3 Result of thermogravimetric measurement of silica-gel fabricated via sol-gel process of TEOS using NH_3 as a catalyst.

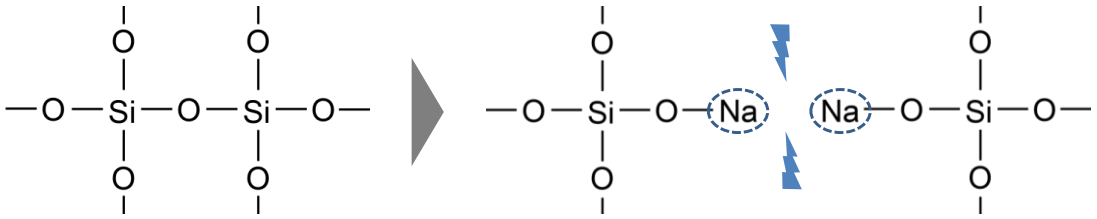

Figure 1.4 Schematic diagram of mechanism of a network modifier in silica network.

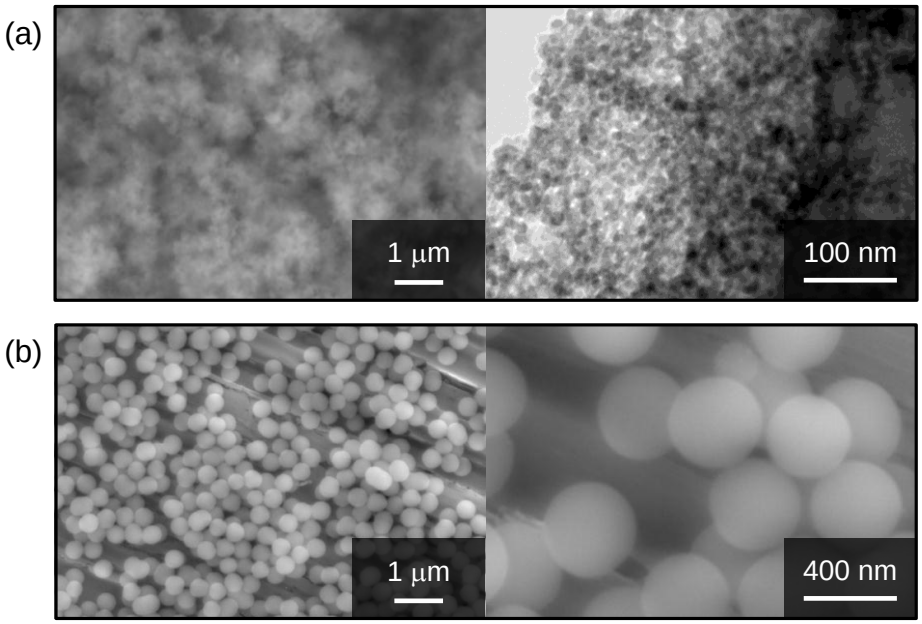

Figure 1.5 FE-SEM images of silica fabricated from TEOS using NaOH aqueous solution (a) and NH_3 aqueous solution (b) as an initiation catalyst.

Figure 1.6 Appearance of glazes of the same pigment with various glass matrices.

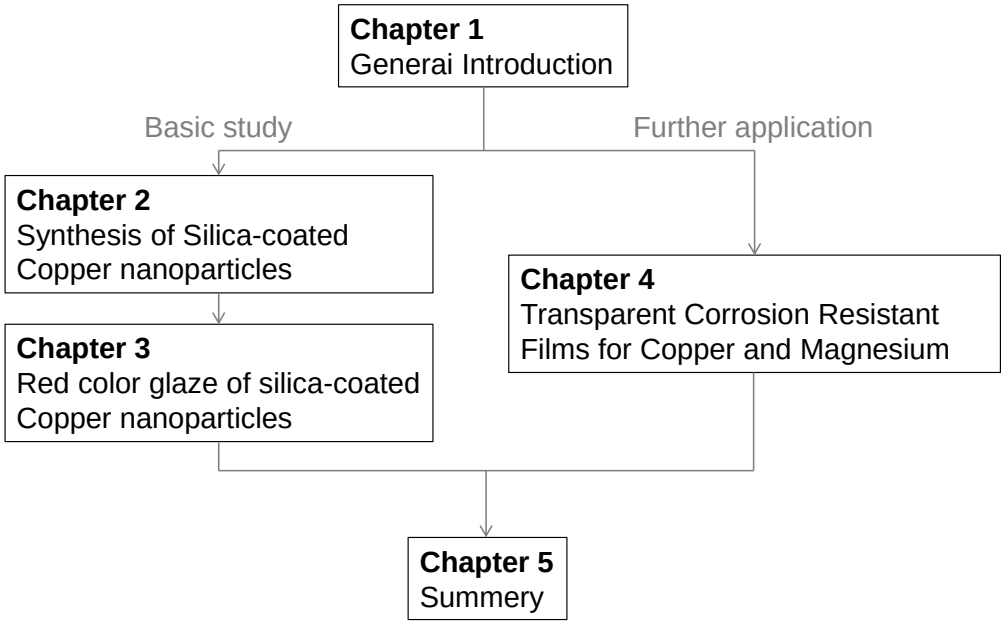

Figure 1.7 Outline of this study.

References

1. A. L. Bacarella1 and J. C. Griess Jr., *J. Electrochem. Soc*., **120**, 459 (1973)
2. J. O'M. Bockris and M. Enyo, *Trans. Faraday Soc*., **58**, 1187 (1962)
3. G. Faita, G. Fiori and D. Salvadore, *Corr. Sci*., **15**, 383 (1975)
4. F. W. Young Jr., J. V. Cathcart and A. T. Gwathmey, *Acta Metall*., **4**, 145 (1956)
5. S. Sun, C. B. Murray, D. Weller, L. Folks, and A. Moser, *Science*, **287**, 1989 (2000).
6. K. Woo, J. Hong, S. Choi, H. W. Lee, J. P. Ahn, C. S. Kim and S. W. Lee, *Chem. Mater.*, **16**, 2814 (2004).
7. A. K. Guptaa and M. Guptab, Biomater., **26**, 3995 (2006).
8. Y. Caiab and R. Tang, *J. Mater. Chem.*, **18**, 3775 (2008).
9. V. Johánek, M. Laurin, A. W. Grant, B. Kasemo, C. R. Henry and J. Libuda, *Science*, **304**, 1639 (2004).
10. U. Backman, U. Tapper and J. K. Jokiniemi, *Synthetic Met*., **142**, 169 (2004).
11. Y. Li, Y. Wu and B. S. Ong, *J. Am. Chem. Soc.*, **127**, 3266 (2005).
12. Y, Lee, J. Choi, K. J. Lee, N. E. Stott and D. Kim, *Nanotechnology*, **19**, 415604 (2008).
13. M. Cho, W. Choi, S. Kim, I. Kim and Y. Lee, *J. Nanosci. Nanotechnol*., **10**, 6888 (2010).
14. A. D. McFarland and R. P. Van Duyne, *Nano Letters*, **3**, 1057 (2003).
15. R. Elghanian, J. J. Storhoff, R. C. Mucic, L. L. Letsinger and C. A. Mirkin, *Science*, **277**, 1078 (1997).
16. S. Magdassi, A. Bassa, Y. Vinetsky and A. Kamyshny, *Chem. Mater.*, **15**, 2208 (2003).
17. A. Gotoh, H. Uchida, M. Ishizaki, T. Satoh, S. Kaga, S. Okamoto, M. Ohta, M. Sakamoto, T. Kawamoto, H. Tanaka, M. Tokumoto, S. Hara, H. Shiozaki, M. Yamada, M. Miyake and M. Kurihara, *Nanotechnology*, **18**, 345609 (2007).

18. E. Bilgili, R. Hamey and B. Scarlett, *Chem. Eng. Sci.*, **61**, 149 (2006).

19. P. Garrigue, M. H. Delville, C. Labrugère, E. Cloutet, P. J. Kulesza, J. P. Morand and A. Kuhn, *Chem. Mater.*, **16**, 2984 (2004).

20. T. Tsuzuki and P. G. McCormick, *J. Mater. Sci*., **39**, 5143 (2004).

21. R. Muszynski, B. Seger and P. V. Kamat, *J. Phys. Chem. C*, **112**, 5263 (2008).

22. X. Wang, J. Zhuang, Q. Peng and Y. Li, *Nature*, **437**, 121 (2005)

23. M. Kogiso, K. Yoshida, K. Yaseb and T. Shimizu, *Chem. Commun*., 2492 (2002).

24. S. Yagi, H. Nakanishi, E. Matsubara, S. Matsubara, T. Ichitsubo, K. Hosoya, and Y. Matsuba, *J. Electrochem. Soc*., **155**, D474 (2008).

25. S. Yagi, T. Koyanagi, H. Nakanishi, T. Ichitsubo, and E. Matsubara, *J. Electrochem. Soc*., **155**, D583 (2008).

26. S. Yagi, M. Kawamori and E. Matsubara, *Electrochemi. Solid St*., **13**, E1 (2010).

27. G. H. Chan, J. Zhao, E. M. Hicks, G. C. Schatz and R. P. Van Duyne, *Nano Lett.*, **7**, 1947 (2007).

28. S. Kapoor, D. K. Palit and T. Mukherjee, *Chem. Phys. Lett*., **355**, 383 (2002).

29. H. H. Huang, F. Q. Yan, Y. M. Kek, C. H. Chew, G. Q. Xu, W. Ji, P. S. Oh and S. H. Tang, *Langmuir*, **13**, 172 (1997).

30. P. Kanninen, C. Johans, J. Merta and K. Kontturi, *J. Colloid Interf. Sci.*, **318**, 88, (2008).

31. W. Stober, A. Fink and E. Bohn, *J. Colloid Interf. Sci.*, **26**, 62 (1968).

32. C.J. Brinker and G.W. Scherer, *J. Non-Cryst. Solids*, **70**, 301 (1985).

33. G. H. Bogush and C. F. Zukoski, *J. Colloid Interf. Sci.*, **142**, 1 (1991).

34. S. Sakka, *Foundation and Application of Glass Science*, Uchida Rokakuho (1997).

35. I. Farnan, P. J. Grandinetti, J. H. Baltisberger, J. F. Stebbins, U. Werner, M. A. Eastman

and A. Pines, *Nature*, **358**, 31 (1992).

36. R. Kernera and J.C. Phillips, *Solid State Commun*., **117**, 47 (2000).

37. H. Takashima, *the Science of Ceramics and Glazes*, Uchida Rokakuho (1994).

38. Y. Yoona, T. Kima, M. Yanga, K. Leea and G. Leeb, *Microchem. J.*, **68**, 251 (2001).

39. H. Takashima, *Practical Science of Pottery*, Uchida Rokakuho (1996).

Chapter 2

Synthesis of Silica-coated Copper Nanoparticles

2.1 Introduction

2.1.1 Cu nanoparticles and silica-coating

As mentioned in the previous chapter, Cu is so sensitive to the ambient atmosphere that it is easily oxidized in air and dissolved into a solution. Cu nanoparticles show the good optical properties such as surface plasmon resonance and they have a characteristic red color, but nanoparticles are much more sensitive to the oxidation and dissolution, since they possess a large specific surface area, and the characteristic red color of Cu nanoparticles is easily spoiled.[1] The difficulty in handling the naked nanoparticles in ambient atmosphere even at room temperature prevents various metal nanoparticles to be easily used. In order to overcome this problem, nanoparticles are often used as composite structures, for example "supported" structure,[2-4] "endohedral" structure,[5,6] or "core-shell" structure.[7-10] Among them, core-shell structure is mostly investigated due to its high stability and dispersibility. In these reports, SiO_2 shell is widely used as it has especially remarkable stability against various chemicals or heat, and it also enables to maintain the unique color and optical property of metal core due to a relatively low refractive index of SiO_2.[11-13] Mine et al. successfully fabricated Au@SiO_2, namely, silica-coated Au nanoparticles, by the sol-gel process using tetraethyl orthosilicate (TEOS) with NH_3 as an initiator of sol-gel process.[11] Moreover, Ag@SiO_2 was fabricated by the similar process by Kobayashi et al.[12] Fabrication of Ag nanowires with conformal sheaths of SiO_2 through a sol-gel process was reported by Yin et al.[13] In the fabrication process of silica-coated metal nanoparticles or nanowires, evaluating

the dissolution behavior of metals and deposition behavior of silica shells is the key to obtain the well coated core-shell structures. However, there is no report on quantitative evaluation of the dissolution and deposition behaviors of target materials for optimizing the reaction bath. Generally the fabrication of $Cu@SiO_2$ nanoparticles is difficult due to the character of Cu nanoparticles which is easily oxidized during the coating process and soluble in NH_3 solutions used as an initiator of sol-gel process. Therefore, control of the reaction bath by the quantitative evaluation of both thermodynamics and kinetics is crucial in the fabrication of $Cu@SiO_2$ nanoparticles.

We have reported the synthesis method of Cu nanoparticles accompanied with electrochemical evaluation.[14] In this synthesis method, Cu nanoparticles are formed by mixing CuO and hydrazine (N_2H_4) in NaOH solution, but in the silica-coating process, NaOH badly affects the formation of silica network. Therefore, in this work, we developed a new synthesis method of Cu nanoparticles which uses NH_3 instead of NaOH, and consistent procedure with a simple beaker method is suggested as shown in Figure 2.1.

2.1.2 Mixed potential measurement

An electrochemical measurement is a powerful tool for monitoring the circumstances around a metal immersed in a solution. Especially, a mixed potential is good indicator of reducing ability in the solution. When a metal is immersed in the solution, two reactions, the oxidation reaction and reduction reaction, simultaneously proceed. These reactions are accompanied with electron transferences, and thus, the electric currents are arisen on the metal. These electric currents are called “anodic current” and “cathodic current”. The balanced potential of total anodic and cathodic currents is called “mixed potential” as

schematically shown in Figure 2.2. By combining the mixed potential and pH measurements with thermodynamic calculations, the most stable species in the solution is estimated. For example, our group has reported that the oxidation-state of Cu is predicted and controlled by comparing the mixed potentials with potential-pH diagrams.[15] Specifically, in this report, the selective synthesis of Cu and Cu_2O nanoparticles was demonstrated by controlling the mixed potential. The difference between the redox potential of metal and the mixed potential corresponds to a driving force of the metal deposition or dissolution, which indicates that we can evaluate the reducing ability of the solution by mixed potentials.

2.1.3 QCM measurement

The information obtained by mixed potential measurements is just a thermodynamic estimation. In other words, we can only know "what is the most stable species in the solution" by mixed potential measurements. Therefore, in order to understand the deposition or dissolution behavior strictly, the kinetic information should be measured in addition to the mixed potential measurements.[16-18] In this work, the behavior of formation and dissolution of metals is investigated by an in-situ QCM measurement in conjunction with the mixed potential measurement. When the deposition or dissolution reaction of metals proceeds in the solution, the similar reaction is detected on the QCM substrate at the same time. The weight change of the QCM substrate Δm was calculated from the frequency of quartz substrate using the following equation (Sauerbrey equation),

$$\Delta m = -\frac{A\sqrt{\rho_q \mu_q}}{2 f_0^{\,2}} \Delta f \qquad (2.1)$$

where f_0 is the frequency of the QCM substrate before the weight change, A is the active area of the QCM substrate (0.196 cm^2), ρ_q is the density of quartz (2.648 g cm^{-3}), and μ_q is the

shear modulus of quartz (2.947×10^{11} g cm^{-1} s^{-2}). As shown in Figure 2.3, the in-situ QCM measurement enables us to evaluate the kinetic information of the deposition or dissolution, such as a reaction rate, a start point, and a terminal point of the deposition and dissolution reaction.

2.1.4 Electrochemical meaning of combination of mixed potential and QCM measurement

In this work, we suggest the concept of evaluating the reducing ability by comparing the measured mixed potential with the oxidation-reduction potential in order to discuss the stability of Cu nanoparticles electrochemically. Figure 2.4(A) schematically shows the mixed potential and pH of the solution plotted against time (red line) and oxidation-reduction potential (blue dot). Figure 2.4(B) is the projection view of Figure 2.4(A), i.e. potential versus time graph. The deposition and dissolution behavior of Cu nanoparticles are properly analyzed accompanied with the QCM measurements. The reduction reaction of Cu formation proceeds as the mixed potential is shifted to be lower than the oxidation-reduction potential by addition of reducing agent. During the precipitation process of Cu, from (a) to (c) in Figure 2.4, the difference between measured mixed potential and oxidation–reduction potential reflects the driving force for the reduction of Cu as shown in (b) in Figure 2.4(B). Since Cu ionic species in the solution momentarily decrease with the precipitation of Cu, the oxidation-reduction potential approaches asymptotically to the mixed potential, and the boundaries of potential-pH diagram change with time. This kinetics of change in oxidation-reduction potential can be evaluated by the termination point in QCM measurement. In other words, the termination point in QCM measurement indicates the completion point of

deposition; (c) in Figure 2.4. The potential-pH diagram is originally drawn for the equilibrium state, however, as Cu gets precipitated, we cannot determine the potential-pH diagram actually. Therefore, at (b), (c) and (d) in Figure 2.4(A), the quasi potential-pH diagrams are drawn over the graph. Cu is kept precipitated as long as the reducing ability is maintained as shown in (c)-(d) in Figure 2.4, however, the mixed potential gradually gets higher by the decomposition of reducing agent with time, and the oxidation-reduction potential follows the mixed potential as shown in (d)-(e) in Figure 2.4, which indicates that Cu is oxidized and then finally dissolved. This dissolution behavior is also expected to be monitored by QCM measurement. The silica-coating should be accomplished before the oxidation of Cu starts, i.e. during the reducing ability is maintained, namely, from (c) to (d) in Figure 2.4. Therefore, we should accurately determine the timing of addition of TEOS for silica-coating by the combined measurement of mixed potential and QCM.

2.2 Experimental

2.2.1 Synthesis method of silica-coated copper nanoparticles

CuO powder is purchased from Kanto Chemical, Inc. Ammonia aqueous solution (NH_3, 28 %), hydrazine monohydrate ($N_2H_4 \cdot H_2O$, 98 %), gelatin fine powder, ethanol (C_2H_5OH, 99.5 %), tetraethyl orthosilicate ($Si(OC_2H_5)_4$, TEOS, 95 %) and nitric acid (HNO_3, 60 %) are purchased from Nacalai Tesque, Inc. and used without further purification.

The whole synthesis procedure is shown schematically in Figure 2.5. The precursor of Cu nanoparticles was first prepared by CuO powder (3.15×10^{-3} mole, 0.25 g) dispersed into NH_3 aqueous solution (28 %, 19 ml) and gelatin (0.20 g) was added as a dispersing agent. Reducing agent solution was also prepared by hydrazine (0.08 mole, 2.0 g) mixed with NH_3

aqueous solution (28 %, 19 ml) and gelatin (0.20 g). These two solutions were agitated separately at a rate of 500 rpm with a magnetic stirrer. The temperature of the solutions was kept at 323 K throughout the reaction for synthesis of Cu nanoparticles. Additionally, the effect of dissolved oxygen was minimized by bubbling nitrogen gas for more than 30 minutes. Then the two solutions were mixed to start the reaction. Here, the total amount of solution is about 40 ml, the molarity of NH_3 is 14.06 mol dm^{-3}, and the molarity of Cu is 0.079 mol dm^{-3}.

In parallel to the above process, ethanol (32 ml) and TEOS (8 ml) was mixed together. The nitrogen gas was also introduced for more than 30 minutes. This solution was added to the synthesized Cu nanoparticles' suspension at room temperature and stirred for more than 20 minutes to fabricate SiO_2 shells on the Cu nanoparticles. Nitrogen gas bubbling was consistently continued through this process. In this procedure, the NH_3 solution works not only as a solvent of Cu nanoparticles, but also as an initiator catalyst of sol-gel process of TEOS.

Finally the product was annealed in Ar gas atmosphere at 973 K for 10 hours to increase the stability of the SiO_2 shells and remove the extra gelatin.

2.2.2 Measurements and characterization

During the reaction, a gold-sputtered QCM electrode (SEIKO EG&G, QA-A9M-AU) or copper-sputtered QCM electrode (SEIKO EG&G, QA-A9M-CU) was immersed in the solution in order to monitor the weight change of the QCM electrode. The weight change was calculated from the frequency of quartz substrate using the Sauerbrey equation. In addition to the QCM measurement, the mixed potential was measured by a potentiostat/ galvanostat

(Hokuto Denko Co., Ltd., HA-151) using an Ag/AgCl electrode (HORIBA, 2565A-10T) as a reference electrode to measure the reducing ability of a solution. The pH of the solution was measured by a pH meter (HORIBA, pH/ COND METER D-54). The morphology of products was observed by a field-emission scanning electron microscope (SEM: JEOL Ltd., JSM-6500F) and a transmission electron microscope (TEM: JEOL Ltd., JEM-2010). The crystalline structure of products was investigated by X-ray diffraction (XRD: Rigaku Corporation, RINT-2500). In the XRD measurement, a soda-silicate glass capillary tube (Hilgenberg GmbH, Markröhrchen aus Glas Nr.10) or a low-background single-crystal silicon sample holder was used to hold the sample.

2.3 Results and Discussions

2.3.1 Deposition and dissolution behavior of Cu nanoparticles

Figure 2.6 shows the time transition in the deposition amount of products on a gold-sputtered QCM electrode and mixed potential during the synthesis process of Cu nanoparticles, namely region 1 in Figure 2.4. The curve of deposition amount is almost flat after 10 minutes, indicating that the reaction is estimated to end in about 10 minutes. This simply means that the mixed potential initially became lower than the oxidation-reduction potential of Cu/Cu(I) redox pair by addition of reducing agent, and after 10 minutes, the concentration of Cu ions decreased and thus the precipitation of Cu nanoparticles finished. The precipitation of Cu nanoparticles was also confirmed by the color change of solution which turned dark red. As shown in Figure 2.6, the precipitation rate of nanoparticles in the reaction bath is evaluated as the deposition on the QCM electrode, indicating that the QCM measurement was applicable to this system.

Figure 2.7 shows the SEM image and the XRD pattern of synthesized Cu nanoparticles. The mean particle size was 30 nm, which was determined by image analysis for randomly selected 300 particles. XRD pattern of the products shown in Figure 2.7(b) indicates that the Cu was evidently synthesized even in NH_3 aqueous solution.

The Cu nanoparticles are kept precipitated as long as the reducing ability is maintained by hydrazine in the solution. However, the lack of the hydrazine, in other words, the decrease of the reducing ability of the solution with time induces the dissolution of Cu nanoparticles. Figure 2.8(a) and Figure 2.8(b) shows the time transition in the thickness of copper-sputtered QCM electrode in the solution during the hydrazine remained, namely, region 2 in Figure 2.4, and after the hydrazine was completely decomposed, namely, region 3 in Figure 2.4. The thickness was calculated from the weight change, Δm, and the density of Cu (8.9 g cm^{-3}). Here, minus indicates the decrease of thickness, i.e. the dissolution of Cu, and the decreasing rate of thickness corresponds to the dissolution rate of Cu nanoparticles. The graph of Cu nanoparticles in region 2, i.e. in the solution with hydrazine, was kept almost flat for 30 minutes as shown in Figure 2.8(a), indicating that the as-synthesized Cu nanoparticles are prevented from dissolution even in NH_3 solution for at least 30 minutes. On the other hand, as shown in Figure 2.8(b), Cu in region 3, i.e. in the solution after the decomposition of hydrazine was continuously dissolved. The two pictures located below the blue line in Figure 2.8(b) are QCM electrode before and after dissolution of Cu, which visually shows the dissolution of Cu on QCM electrode. Considering the diameter of synthesized Cu nanoparticles of about 30 nm, Cu nanoparticles are estimated to be completely dissolved within 1 minute in the solution without hydrazine. The difference in the dissolution rate is concerned with the reducing ability of the solution. The reducing ability of the solution could

be evaluated from a measurement of mixed potential. The mixed potential is determined as the balanced potential of total anodic currents and total cathodic currents induced by anodic and cathodic reactions. In this suspension, oxidation of hydrazine and oxidation of Cu are considered to proceed as main anodic reactions shown in equations (2.2), (2.3), and reduction of dissolved oxygen as a cathodic reaction shown in equation (2.4).

$$N_2H_4 + 4OH^- \rightarrow N_2 + 4H_2O + 4e \quad (2.2)$$

$$Cu \rightarrow Cu(I) + e \quad (2.3)$$

$$O_2 + 4e + 2H_2O \rightarrow 4OH^- \quad (2.4)$$

Figure 2.8(c) shows the time transition in the mixed potentials in the as-synthesized Cu nanoparticles' suspension, and Figure 2.8(d) shows the time transition in the mixed potentials in the solution after Cu nanoparticles was completely dissolved. The dotted line in Figure 2.8(c) and Figure 2.8(d) is the oxidation–reduction potential, *E*, of Cu/Cu(I) redox pair (−0.30 V vs SHE) calculated from the thermodynamic data listed in table 1,[19] where the measured pH of the solution is 12.9 and the total concentration of Cu(I) ionic species is assumed as the total amount of Cu chemical species contained in the solution (0.079 mol dm^{-3}). In the as-synthesized Cu nanoparticles' suspension, the existence of hydrazine maintained the reducing ability of solution, which could be verified from the lower mixed potential than the oxidation–reduction potential of Cu/Cu(I) redox pair as shown in Figure 2.8(c). This is consistent with the result of QCM measurement that Cu nanoparticles are prevented from dissolution for at least 30 minutes as shown in Figure 2.8(a). While, the mixed potential of copper-dissolved NH_3 aqueous solution bath is higher than the oxidation–reduction potential of Cu/Cu(I) redox pair as shown in Figure 2.8(d), indicating that Cu metal is dissolved into this solution, which is consistent with the dissolution behavior shown in Figure 2.8(b).

2.3.2 SiO_2 coating of Cu nanoparticles

Figure 2.9 shows the time transition in the deposition amount of products on a QCM electrode during the fabrication of SiO_2. The change in the deposition amount is almost flat after 20 minutes, and thus the reaction is estimated to end in about 20 minutes. As the synthesized Cu nanoparticles are kept at least 30 minutes with the residual hydrazine as shown in figure 2.9(a), the SiO_2 shells were sufficiently formed before the dissolution of Cu nanoparticles.

Figure 2.10 shows the SEM image and the XRD pattern of synthesized Cu@SiO_2 nanoparticles. Cu nanoparticles remains in SiO_2 shell and thickness of SiO_2 shell is about 40-50 nm.

In order to increase the stability of SiO_2 shells and to remove the extra gelatin, Cu@SiO_2 nanoparticles were annealed in Ar gas atmosphere at 973 K. Figure 2.11 shows the TEM image and the XRD pattern of Cu@SiO_2 nanoparticles after annealing process. The sample was held on a low-background single-crystal silicon sample holder for XRD measurement. As shown in Figure 2.11, Cu nanoparticles remained in SiO_2 shells and the thickness of SiO_2 shell decreased to about 30-40 nm, indicating the SiO_2 shells were condensed and tightened by the annealing process.

To check the stability of the annealed sample, both annealed and non-annealed product were immersed in 1.0 mol dm^{-3} HNO_3 aqueous solution, which is known as a strong oxidizing agent. Figure 2.12 shows the TEM image and XRD pattern of annealed and non-annealed Cu@SiO_2 nanoparticles which were immersed in HNO_3 for 24 hours. The annealed SiO_2 shells prevented Cu nanoparticles from oxidation and dissolution, and

$Cu@SiO_2$ nanoparticles stayed unchanged even in a strong oxidizing agent as shown in the TEM image (i) in Figure 2.12(a). On the other hand, the Cu in non-annealed $Cu@SiO_2$ nanoparticles was dissolved into HNO_3 aqueous solution and hollow SiO_2 particles are obtained as shown in TEM image (ii) in Figure 2.12(a). These results are also confirmed by the XRD pattern shown in figure 2.12(b).

2.4 Conclusions

In this chapter, we have demonstrated the synthesis method of silica-coated Cu nanoparticles and suggested the technique for evaluating the dissolution behavior of Cu using mixed potentials and QCM measurements. Cu nanoparticles were synthesized via electroless deposition method in a NH_3 aqueous solution, and we have verified that it takes about 10 minutes for precipitating Cu nanoparticles by monitoring the deposition rate. If Cu is dispersed in the NH_3 solution, Cu is continuously dissolved into NH_3 solution by forming ammine complexes. However, in this work, reducing ability of the solution was maintained by the hydrazine and Cu nanoparticles were stably dispersed in the solution bath for at least 30 minutes. On the other hand, SiO_2 shells were fabricated by sol-gel process of TEOS. The formation rate of SiO_2 was also verified by QCM measurement. SiO_2 shells were fabricated much faster than the dissolution rate of Cu nanoparticles, which is important for the fabrication of well coated Cu nanoparticles.

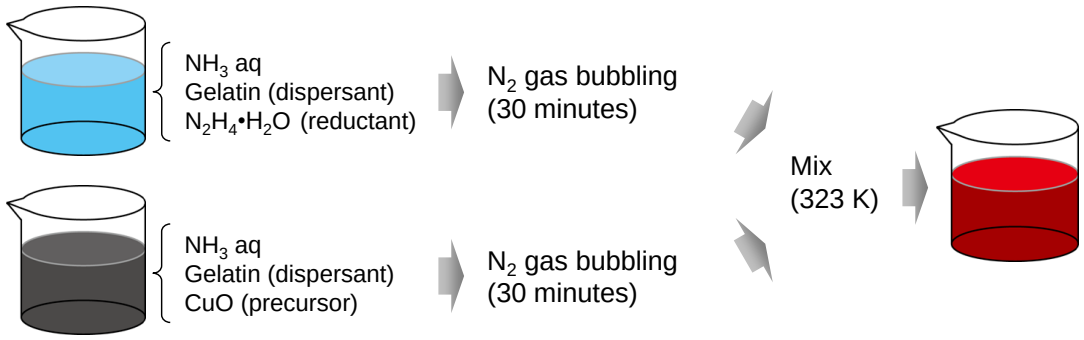

Figure 2.1 Schematic illustration of procedure for synthesis of Cu nanoparticles.

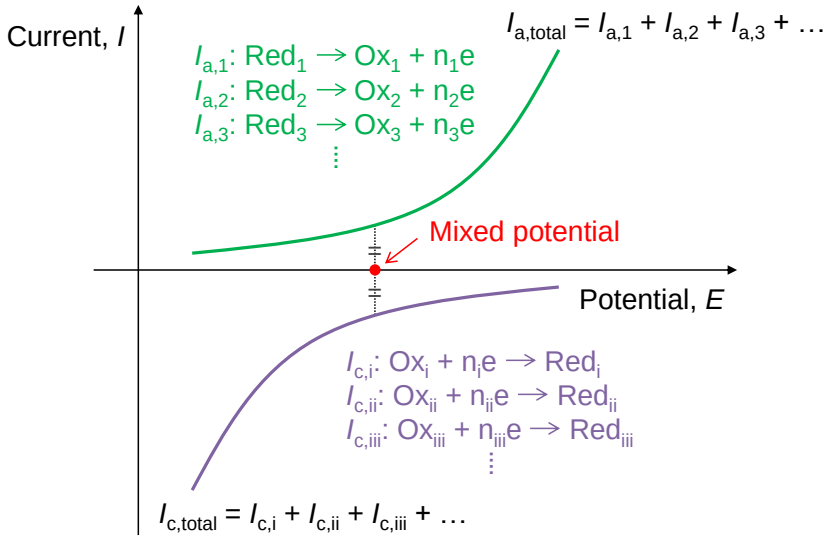

Figure 2.2 Schematic illustration of relation of anodic and cathodic currents with mixed potential.

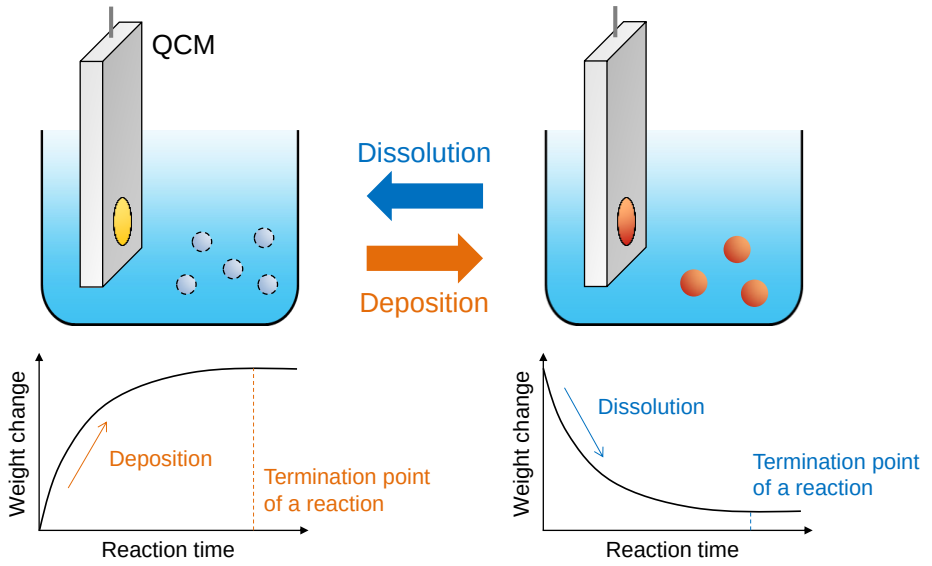

Figure 2.3 Conseptual diagrams of QCM measurement and weight change graphs detected by QCM measurement during deposition and dissolution reaction.

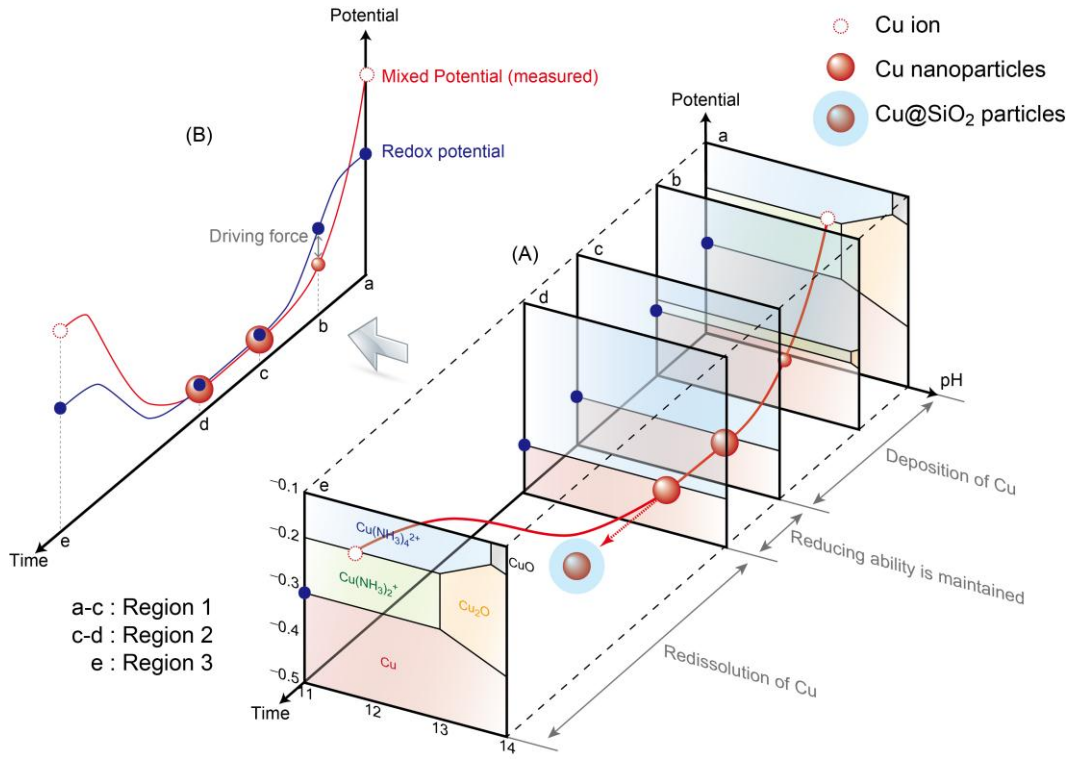

Figure 2.4 Schematic diagram of the time transition in the mixed potential and oxidation-reduction (redox) potential, overdrawn on the time-dependent quasi potential-pH diagrams.

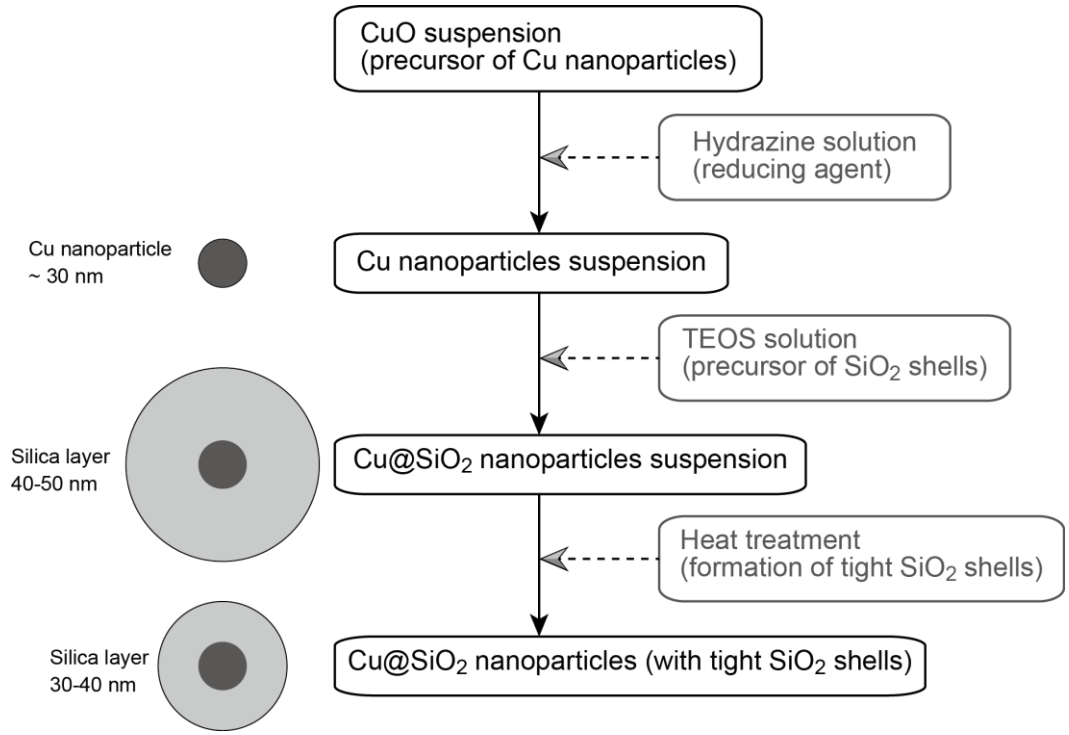

Figure 2.5 Schematic diagram of the whole procedure for synthesis of silica-coated Cu nanoparticles.

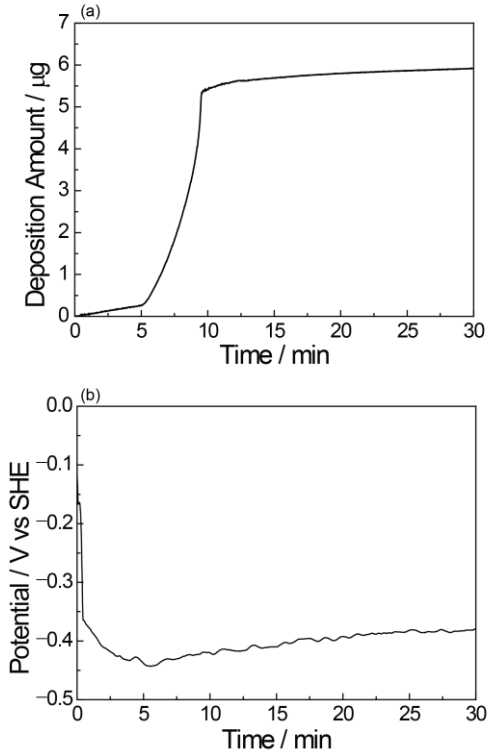

Figure 2.6 Time transition in (a) deposition amount of Cu deposited on a QCM electrode and (b) mixed potential during the synthesis of Cu nanoparticles.

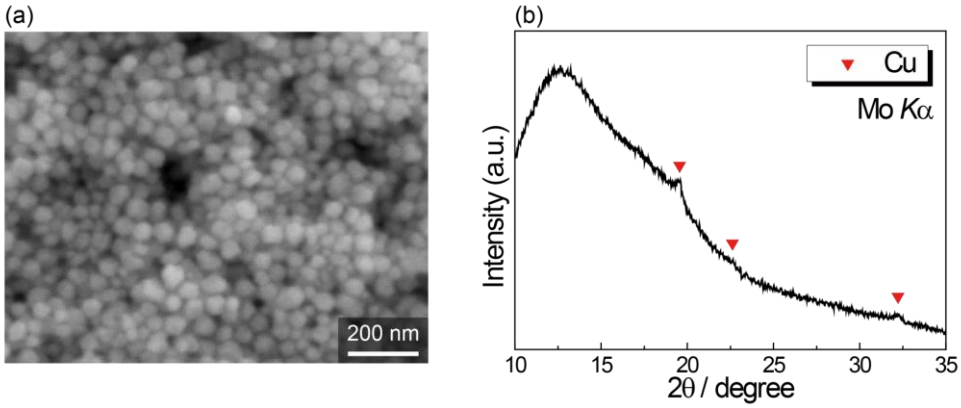

Figure 2.7 (a) SEM image of Cu nanoparticles and (b) XRD pattern of Cu nanoparticles held in a capillary tube.

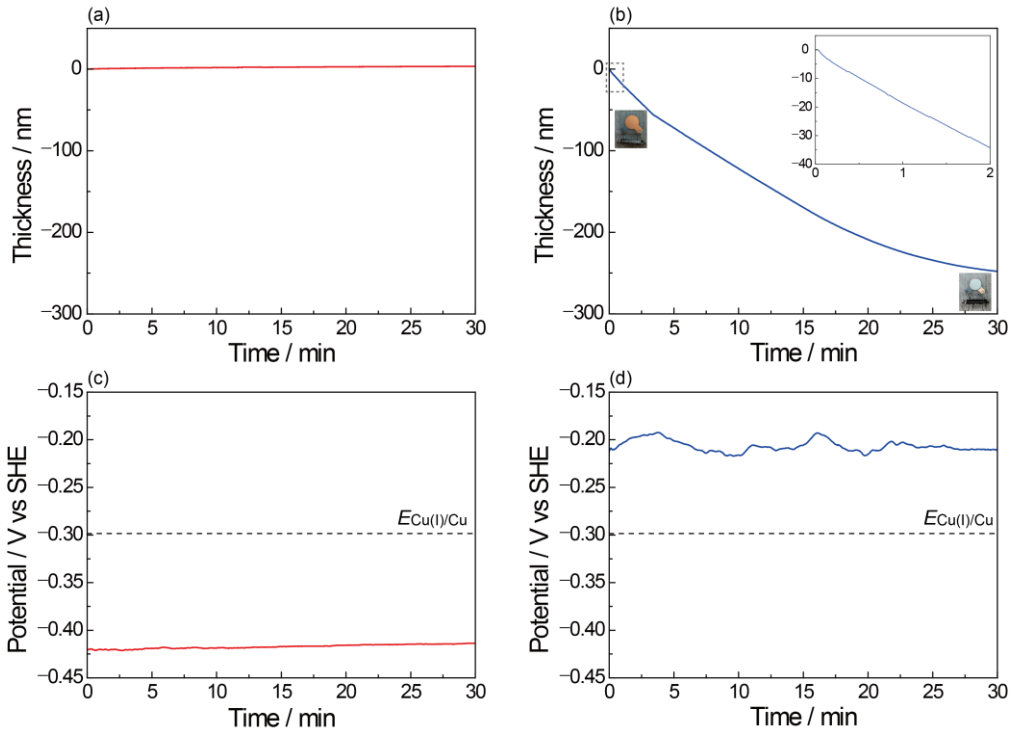

Figure 2.8 Time transition in the thickness of copper-sputtered QCM electrodes immersed in Cu nanoparticles' suspension (a) during the reducing ability was maintained (region 2) and (b) after the dissolution of Cu nanoparticles (region 3), (c) mixed potential in the Cu nanoparticles' solution measured at the same time as (a), and (d) mixed potential in the Cu nanoparticles' solution measured at the same time as (b).

Table 2.19 The molar chemical potentials used in the calculations.[19]

Substance	μ^0 (kcal/mol)	Substance	μ^0 (kcal/mol)
H^+	0	Cu	0
NH_3	−6.36	Cu^+	12.00
NH_4^+	−19.0	$Cu(NH_3)_2^+$	−15.6
H_2O	−56.69	$Cu(NH_3)^+$	−2.8
NH_4OH	−62.86		

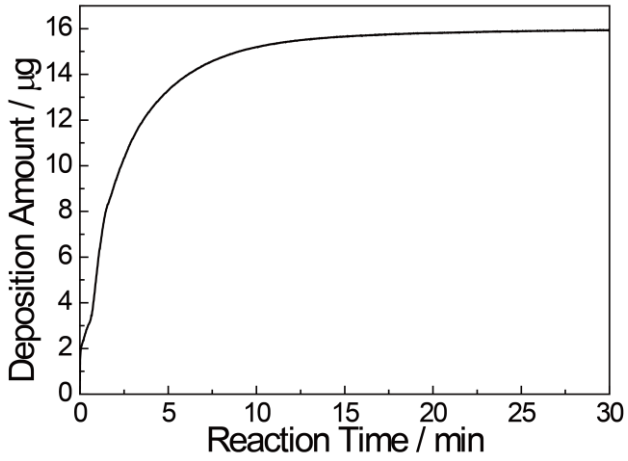

Figure 2.9 Time transition in the deposition amount of silica on a QCM substrate during the fabrication of silica shells.

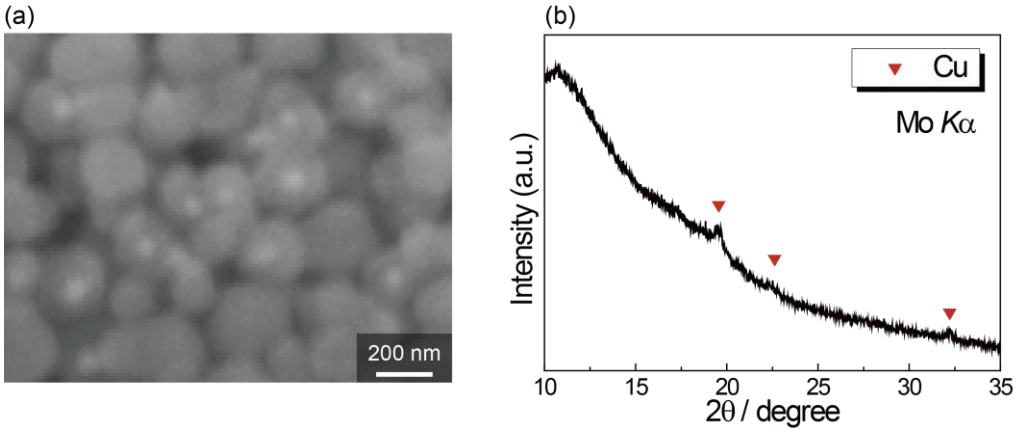

Figure 2.10 (a) SEM image and (b) XRD pattern of non-annealed Cu@SiO_2 core-shell particles held in a capillary tube.

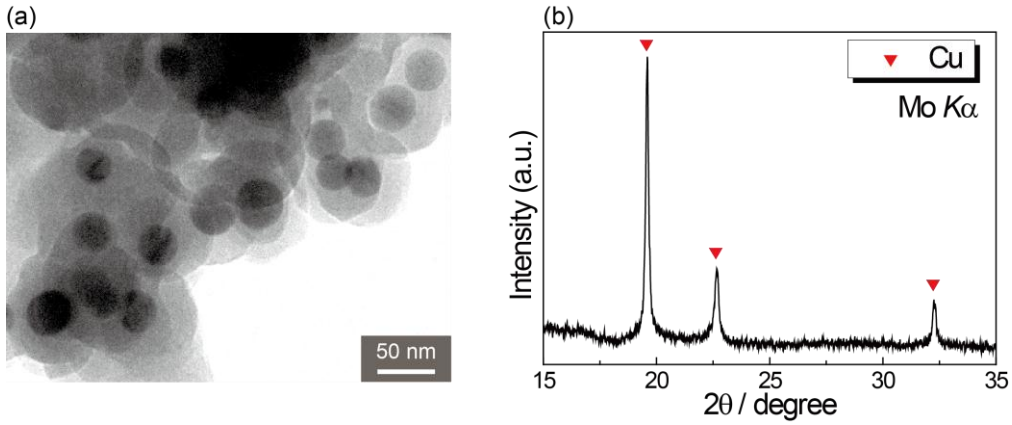

Figure 2.11 (a) TEM image and (b) XRD pattern of Cu@SiO_2 core-shell particles which were annealed to form tight SiO_2 shells.

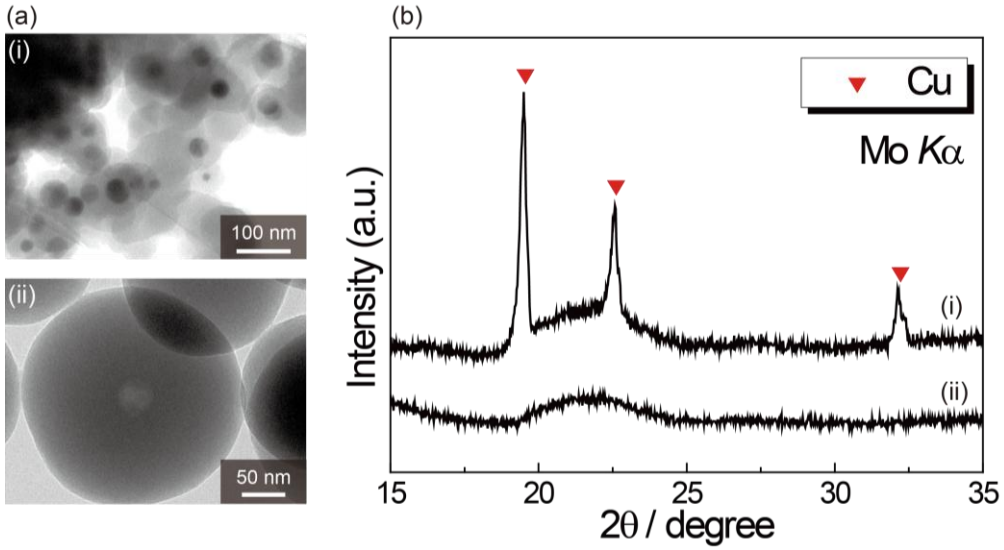

Figure 2.12 (a) TEM image and (b) XRD pattern of (i) annealed Cu@SiO_2 particles immersed in HNO_3 and (ii) Cu@SiO_2 particles without annealing process immersed in HNO_3.

References

1. S. Jeong, K. Woo, D. Kim, S. Lim, J. S. Kim, H. Shin, Y. Xia and J. Moon, *Adv. Funct. Mater*., **18**, 679 (2008).
2. J. B. Park, J. Graciani, J. Evans, D. Stacchiola, S. D. Senanayake, L. Barrio, P. Liu, J. F. Sanz, J Hrbek and J. A. Rodriguez, *J. Am. Chem. Soc*., **132**, 356 (2010).
3. J. Ding, K. Y. Chan, J. Ren and F. Xiao, *Electrochim. Acta*, **50**, 3131 (2005).
4. L. M. Molina1, M. D. Rasmussen1 and B. Hammer, *J. Chem. Phys*., **120**, 7673 (2004).
5. R. Tenne, M. Homyonfer and Y. Feldman, *Chem. Mater.*, **10**, 3225 (1998).
6. M. Yamada, T. Akasaka and S. Nagase, *Acc. Chem. Res*., **43**, 92 (2010).
7. X. Teng, D. Black, N. J. Watkins, Y. Gao and H. Yang, Nano Letters, **3**, 261 (2003).
8. R. T. Tom, A. S. Nair, N. Singh, M. Aslam, C. L. Nagendra, R. Philip, K. Vijayamohanan and T. Pradeep, *Langmuir*, **19**, 3439 (2003).
9. Y. P. He, S. Q. Wang, C. R. Li, Y. M. Miao, Z. Y. Wu and B. S. Zou, *J. Phys. D: Appl. Phys*., **38**, 1342 (2005).
10. Y. Lu, Y. Yin, Z. Y. Li and Y. Xia, *Nano Lett.*, **2**, 785, (2002).
11. E. Mine, A. Yamada, Y. Kobayashi, M. Konno and L. M. Liz-Marzán, *J. Colloid Interf. Sci.*, **264**, 385 (2003).
12. Y. Kobayashi, H. Katakami, E. Mine, D. Nagao, M. Konno and L. M. Liz-Marzán, *J. Colloid Interf. Sci.*, **283**, 392 (2005).
13. Y. Yin, Y. Lu, Y. Sun and Y. Xia, *Nano Lett*., **2**, 427 (2002).
14. S. Yagi, H. Nakanishi, E. Matsubara, S. Matsubara, T. Ichitsubo, K. Hosoya and Y. Matsuba, *J. Electrochem. Soc.*, **155**, D474 (2008).
15. S. Yagi, H. Nakanishi, T. Ichitsubo and E. Matsubara, *J. Electrochem. Soc.*, **156**, D321

(2009).

16. S. Yagi, M. Kawamori and E. Matsubara, *Electrochem. Solid St.*, **13**, E1 (2010).
17. S. Yagi, M. Kawamori and E. Matsubara, *J. Electrochem. Soc.*, **157**, E92 (2010).
18. M. Kawamori, S. Yagi and E. Matsubara, *J. Electrochem. Soc.*, **159**, E37 (2012).
19. W. M. Latimer, *The Oxidation States of the Elements and Their Potentials in Aqueous Solutions, 2nd ed.*, Prentice-Hall, Englewood Cliffs, (1959).

Chapter 3

Red Color Glaze of Silica-coated Copper Nanoparticles

3.1 Introduction

3.1.1 Red color glaze using copper

Since ancient times, red glass, especially transparent and deep red glass, has been always desired. In terms of glaze, which covers potteries or dishes, not only color quality or performance but also environmental and human safety is highly required. For these reasons gold or copper has often been used as a pigment of red color glass and glaze.[1-3] For example, in Kyoto, Japan, a technique of manufacturing the oxblood (deep red) glaze called *shinsha*, using copper, has been traditionally developed by many craftworkers.[4] Oxblood glaze is the high-temperature glaze which is generally achieved by means of heat-treating glass materials with metallic copper or copper oxide under reducing atmosphere. In that process, carbon monoxide (CO) gas flow and high temperature are necessary in order to achieve red color, so it is considered that oxblood glaze is one of the most dangerous and difficult glazes. If the appropriate condition is not provided, the color of glaze becomes blue or green after firing as shown in Figure 3.1. Furthermore, to provide more beautiful red color, Pb is often added to the glaze,[5-7] and thus, these glazes may badly affect the human health. In silicate glass, five types of copper components, metallic copper (Cu), copper oxides (Cu_2O, CuO) and copper ionic species coordinated by oxygen atoms (Cu^+, Cu^{2+}), can be considered to exist. Among these components, only Cu and Cu_2O are capable of coloring glass redly, and the others do not work as red ingredients, so copper should not be oxidized to CuO or ionic species when red color is needed. In other words, if Cu or Cu_2O can be stably dispersed in glazes through

the heat-treatment for melting and shape-forming on potteries or ceramics, red color is achieved dramatically easily compared with current method.

In this work, we propose a safe and easy red color glaze for overglaze decoration by using silica-coated copper nanoparticles. The stable silica-shells sufficiently protect the Cu nanoparticles and prevent them from oxidation even during the heat-treatment, which means that the CO gas flow and the addition of Pb become needless in this concept.

3.1.2 Pb-free low-melting-point glass frit (*raku*-frit)

As mentioned in the first chapter, glass frits are often used for the overglazing as the low-temperature glaze. For lowering the melting point of glass, the addition of alkali and alkaline-earth metal components is indispensable, since they work as a network modifier in the glass network. In terms of glazes, not only lowering the melting point but good adhesion property to a green body of ceramics is also important. The addition of PbO is also effective to stabilize the glass network and lower the melting point. It is reported that both network former like and network modifier like PbO can exist in the glass network, and other additive elements influence the function of Pb. Therefore, Pb has been known as the useful element and widely used until now. However, recently, with increasing the attention to health and reinforcing the legal regulation, the Pb-free products are intensively desired.[8]

In Kyoto Municipal Institute of Industrial Technology and Culture, the research for the Pb-free low-melting-point glass frit has been investigated for several years, and Pb-free glass frit called *raku*-frit which has low melting point of 953 K was produced. This new glass frit widely attracts a great attention in the ceramics industry due to its low melting point, good adhesion property to a green body of ceramics, and high safety. In this work, we use this

raku-frit to fabricate the glaze of silica-coated Cu nanoparticles and follow the same glazing procedure as the testing method taken in Kyoto Municipal Institute of Industrial Technology and Culture. The component of *raku*-frit is listed in Table 3.1.[9]

3.1.3 Color value in L*a*b* color space

In this study, the evaluation of color is significantly important because the purpose of this work is "red color" of glaze. A color value of a color space is a good tool for the quantitative evaluation of color. A color space is a stereoscopically visualized space of color system, which enables us the description of color by the coordinate value. Various configuration models of color space are suggested in the world, for instance, Munsell model, RGB model, XYZ model, and L*a*b* model.[10,11] The L*a*b* color model is based on the human perception, and it is possible to evaluate the difference of colors by determining the distance between two points in the color space. Figure 3.2 shows the color space of L*a*b* color model. L* value corresponds to the lightness (L* = 0 indicates black and L* = 100 indicates diffuse white), and a* and b* value correspond to the colors (a* = negative values indicate green, a* = positive values indicate red, b* = negative values indicate blue and b* = positive values indicate yellow). In this work, the color of fabricated glaze is quantified and evaluated by L*a*b* color model measured by a colorimeter.

3.2 Experimental

The *raku* frit, namely Pb-free low-melting-point glass frit, was provided by Kyoto Municipal Institute of Industrial Technology and Culture. The silica-coated Cu nanoparticles which were tightened by heat-treating at 1173 K in Ar atmosphere were prepared by the same

method as described in chapter 2. Silicon (Si) powder was purchased by Wako Pure Chemical Industries, Ltd.

The *raku* frit (1.0 g) and silica-coated Cu nanoparticles (0.04 g) were mixed in a mortar without and with Si powder (0.003 g, 0.005 g). The mixture was put on white ceramic test pieces, and heat-treated in a temperature profile like figure 3.3 under ambient atmosphere.

The color of fabricated glaze was quantified by a colorimeter (Nippon Denshoku, NF333 spectrophotometer).

3.3 Results and Discussions

Figure 3.4 shows the measured color value of the *shinsha* glaze, which is set as the target color in this study. Figure 3.5 shows the cross-sectional microscopic image of the *shinsha* glaze. As shown in Figure 3.5, the bluish glass layer covers on the red foundation layer, and this bluish layer is the key of the characteristic deep red color of *shinsha* glaze. When the surface blue layer is polished, the bright red color appears as shown in Figure 3.6.

Figure 3.7 shows the appearances and color values of fired glazes. For comparison, the appearance of fired glaze of raw Cu nanoparticles which is not coated is shown in Figure 3.8. In Figure 3.7, the distance on the L*a*b* color space indicates the difference of color, and in this work, the sample which has the nearest color to the *shinsha* glaze is 0.003 g-Si-added sample. This indicates that Si controls the oxidation of Cu nanoparticles, but the excess addition badly affects the final color of fired product. The sample which does not contain Si powder also shows the red color, which indicates the silica-shells efficiently protect the Cu nanoparticles even against the attack of oxygen in firing process of glaze. In this result, even the color of 0.003 g-Si-added sample was yet a little different from the deep red color of

shinsha glaze. However, the characteristic deep red color of *shinsha* glaze can be caused by the blue layer on the top of the glaze, and thus, the target color is considered to be achieved by further ingenuity, for example, extending the firing time, rising the firing temperature, or quantitative control of cooling profile.

3.4 Conclusions

In this chapter, we have achieved the red color glaze for the application of Cu@SiO_2 nanoparicles. The silica-shells effectively protect the Cu from oxidation in the firing process of 1073 K, and red color glaze is produced even without any additional agents. The sample which has the nearest color to *shinsha* glaze is 0.003 g-Si-added sample, which indicates the addition of Si is effective to control the oxidation of Cu. Even this sample showed a little different color from *shinsha* glaze, but the characteristic deep red color of *shinsha* glaze is due to the blue layer on the glaze, and thus there may be some approaches to achieve better red color.

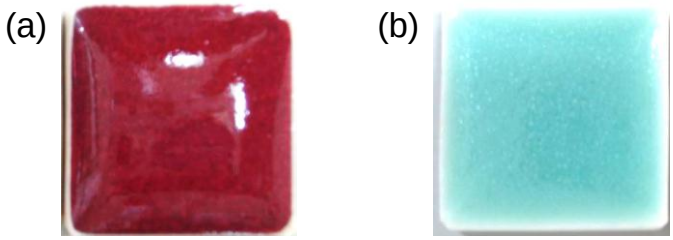

Figure 3.1 Appearances of glaze which contains Cu fired (a) in reducing atmosphere and (b) in air.

Table 3.1 Components of *raku*-frit.[9]

Component	Molar fraction
SiO_2	60.0 – 66.0 %
Al_2O_3	2.0 – 4.0 %
B_2O_3	12.0 – 26.0 %
Li_2O	0 – 10.0 %
Na_2O	1.5 – 5.0 %
K_2O	2.5 – 5.0 %
CaO	0 – 1.0 %
MgO	0 – 1.0 %
SrO	0 – 1.0 %
BaO	0 – 2.5 %
ZnO	1.0 – 8.0 %

$SiO_2 + Al_2O_3$: 63 – 68 %

$B_2O_3 + R_2O + RO$: 32 – 37 %

$R_2O + RO$: 8.5 – 24.5 %

$R_2O > RO$

$$\frac{Li_2O}{Na_2O + K_2O} < \frac{4}{3}$$

$$\frac{CaO + MgO + SrO}{BaO + ZnO} < \frac{2}{3}$$

($R_2O = Li_2O + Na_2O + K_2O$)
(RO = CaO + MgO + SrO + BaO + ZnO)

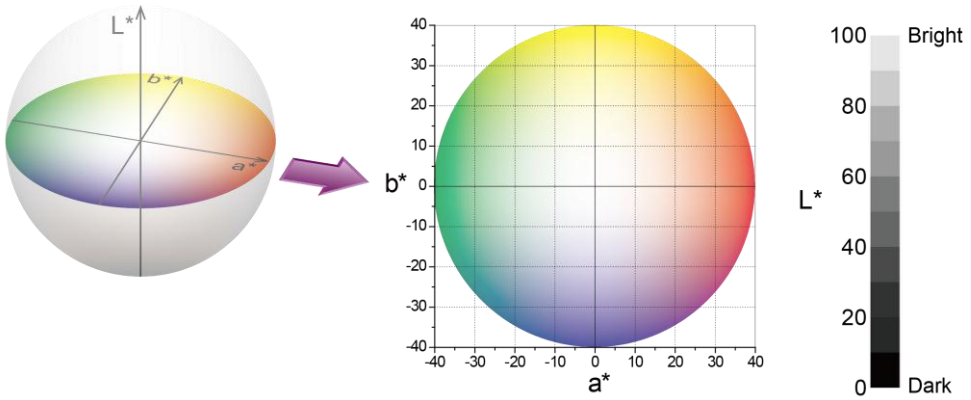

Figure 3.2 Schematic illustration of L*a*b* color space and its cross-sectional diagram of a*b* plane.

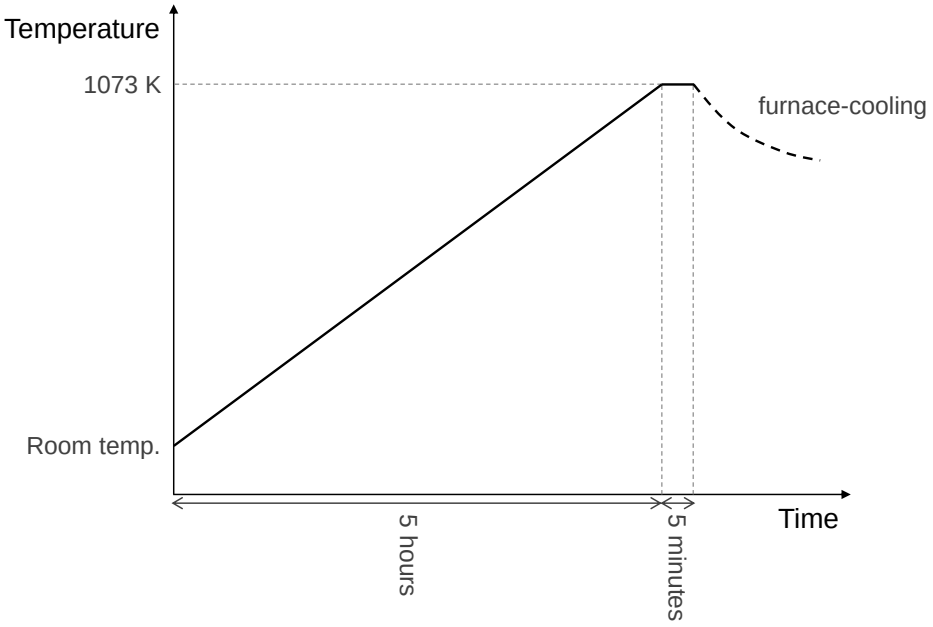

Figure 3.3 Temperature profile of firing glazes.

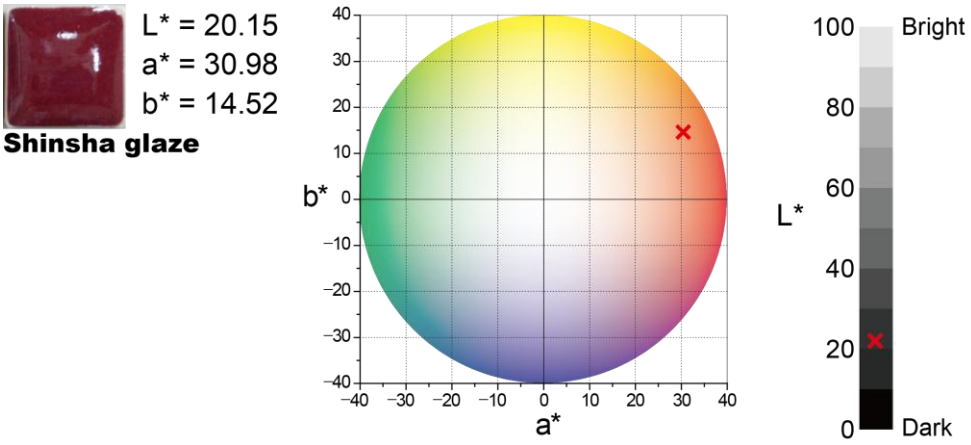

Figure 3.4 Color value of *shinsha* glaze.

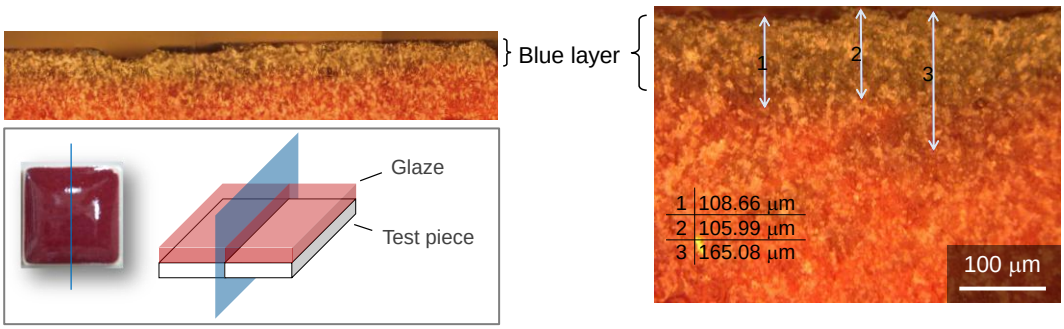

Figure 3.5 Cross-sectional microscopic image of *shinsha* glaze.

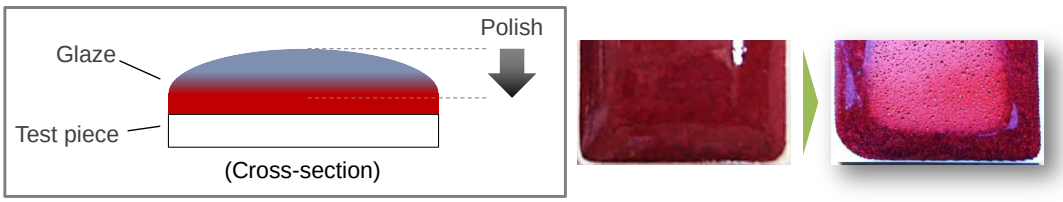

Figure 3.6 Bright red color of polished *shinsha* glaze.

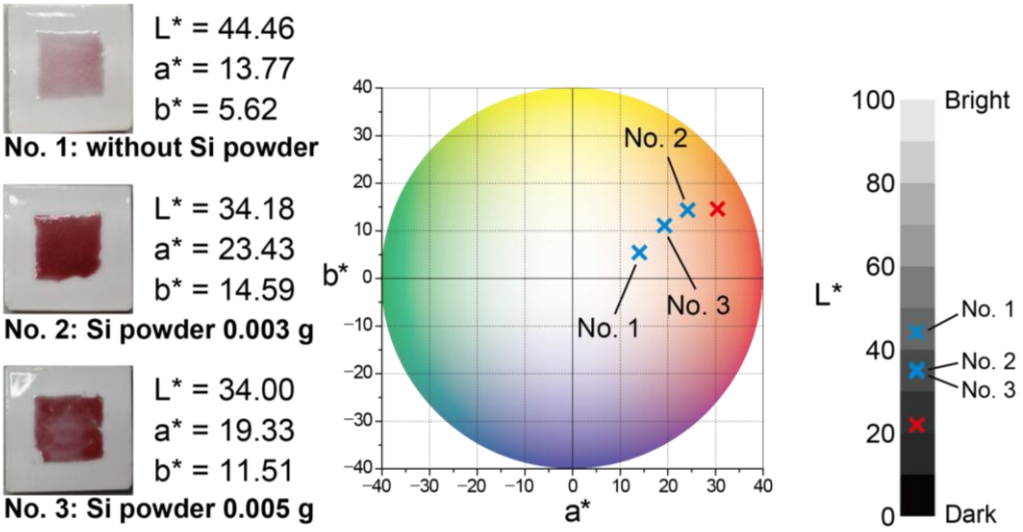

Figure 3.7 Color values of fired glazes of silica-coated Cu nanoparticles.

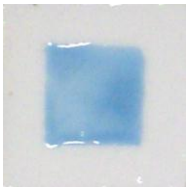

Figure 3.8 Appearance of fired glazes of raw Cu nanoparticles.

References

1. S. F. Brown and F. H. Norton, *J. Am. Ceram. Soc.*, **42**, 499 (1959).
2. J. Lafait, S. Berthier, C. Andraud, V. Reillon and J. Boulenguez, *C. R. Phys.*, **10**, 649 (2009).
3. P. Colomban, *J. Nano Res*., **8**, 109 (2009).
4. M. Wakamatsu, N. Takeuchi and S. Ishida, *J. Non-Cryst. Solids*, **80**, 412 (1986).
5. S. Padovani, C. Sada, P. Mazzoldi, B. Brunetti, I. Borgia, A. Sgamellotti, A. Giulivi, F. D'Acapito and G. Battaglin, *J. Appl. Phys*., **93**, 10058 (2003).
6. M.O. Figueiredo, T.P. Silva and J.P. Veiga, *Appl. Phys. A*, **83**, 209 (2006).
7. J. Roquéa, J. Molerab, P. Sciauc, E. Pantosd and M. Vendrell-Saza, *J. Eur. Ceram. Soc*., **26**, 3813 (2006).
8. L.M. Schabbach, F. Andreola, I. Lancellotti and L. Barbieri, *Ceram. Int*., **37**, 1367 (2011).
9. K. Imai and T. Yokoyama, *Lead-Free Frit for Japanese Coloring Material for Pottery and Lead-Free Japanese Coloring Material for Pottery Containing the Frit* (09-100182), Japanese Patent (Publication in 1997).
10. D. Sarac, Y. S. Sarac, E. Yuzbasioglu and S. Bal, *J. Prosthet. Dent*., **96**, 122 (2006).
11. M. Martos, M. Martínez, E. Cordoncillo and P. Escribano, *J. Eur. Ceram. Soc*., **27**, 4561 (2007).

Chapter 4

Transparent Corrosion Resistant Films for Copper and Magnesium

4.1 Introduction

4.1.1 Improvement in corrosion resistance of metals

A passivation film formed in wet condition around room temperature is generally hydrated oxide, oxyhydroxide or insoluble compound of a substrate metal.[1-3] Ti, Al, stainless steel, etc. typically form the tight and thin layers with a few nm thicknesses, and thus they have transparent passivation films. On the other hand, Mg, Cu, Zn, Pb, etc. form the thick layers, and thus they are tarnished. In terms of Mg, we have tried the plasma anodization for improvement of corrosion resistance, and we have found that the glassy coating layer is formed on the Mg substrate and relatively high corrosion resistance is achieved by the plasma anodization.[4,5] Currently, to achieve the practical use of Mg, transparent coating with high stability is needed. However, the coated layer formed by plasma anodization is thick and whitish appearance. Therefore, to fabricate the transparent coating layer, a different coating method should be investigated.

In this work, we focused the sol-gel dip coating for the improvement of corrosion resistance of metals.[6,7] By taking the appropriate way of sol-gel dipping process, thin and transparent coating layers can be achieved and shiny appearances of metals are maintained. Moreover, since the sol-gel process proceeds at relatively low temperature, the coated metals are scarcely damaged by heat. Therefore, the sol-gel dip coating is adequate method for fabricating the coating layer on a metal which is sensitive to the oxidation and corrosion.

4.1.2 Modified solution of sol-gel process for dip coating of bulk materials

The preparation of appropriate sol-gel solution is one of the most important factors to fabricate the uniform coating layer with good adhesion property and no cracks. The process of dip coating is simply represented by three steps; dipping, withdrawal and drying, and the silica coating layer is formed with the drying process of the solution on the substrate.[8] Therefore the sol-gel solution should not be entirely reacted before drying. Moreover, since the silica coating layer gets hard and tight as the dehydration reaction and condensation reaction proceed, cracks are often generated during the drying process or heat-treatment. In order to overcome this problem, trifunctional alkoxysilane like aminopropyl triethoxysilane (APTES) or phenyl triethoxysilane (PhTES) is often used.[9,10] Tetrafunctional alkoxysilane like TEOS has four alkoxy groups, namely, four reactive functional groups, and thus the strong network with four bonds per one Si atom can be constructed. On the other hand, trifunctional alkoxysilane has only three reactive functional groups, and the network is modified by the unreactive functional groups. This modified network contributes the flexibility of fabricated silica layer and controls the emergence of cracks. In this work, we choose APTES as the coating solution. In addition to the contribution of APTES for flexibility, good adhesion property to the substrate metal is expected due to the amino group in APTES.[11]

4.1.3 Evaluation of corrosion resistance

To evaluate the corrosion resistance, various evaluation techniques are suggested, for example, exposure test,[12,13] immersion test,[14,15] spray test[16,17] and electrochemical test including cyclic voltammetry, polarization curve measurements, electrochemical impedance

spectroscopy, etc.[18-20] By the exposure test and the immersion test, actual information can be provided, based on the practical corrosion environment. However, these tests need much time to wait the corrosion in a practical environment. Therefore, accelerated corrosion tests are widely developed. Salt spray test is one of the famous methods in the spray tests. It is a typical accelerated corrosion test that produces a corrosive attack to the coated samples in order to predict its suitability in use as a protective finish. Also, the electrochemical test is often used for measuring the stability against the corrosion in a solution. Since the corrosion reaction is accompanied with the electron transfer, electrochemical analyses are important and powerful tool to evaluate the corrosion behavior. Among them, Tafel extrapolation method and polarization resistance measurement are commonly used for the quantitative evaluation of corrosion resistance property.[21,22]

4.2 Experimental

4.2.1 Silica-coating of bulk copper and magnesium

Copper plate (B-60-P05) was purchased from YAMAMOTO MS Co., Ltd. Magnesium plate (MG-273408, 99.9 %) was purchased from The Nilaco Corporation. Ethanol (C_2H_5OH, 99.5 %), aminopropyl triethoxysilane ($Si(OC_2H_5)_3(CH_2)_3NH_2$, APTES, 98 %), acetone ($(CH_3)_2CO$, 99.5 %), citric acid ($C_3H_4(OH)(COOH)_3$, 99 %), nitric acid (HNO_3, 60 %) and sodium chloride (NaCl, 99.5 %) were purchased from Nacalai Tesque, Inc. and used without further purification.

The sol-gel solution for coating was prepared by APTES (5 g) and ethanol (20 g) stirred together for 1 day at a rate of 500 rpm with a magnetic stirrer in room temperature. Cu plate was cut in 15 × 50 mm and washed by acetone, then immersed in 5 wt% citric acid solution

for surface cleaning. The cleaned Cu plate was dipped into the APTES-ethanol solution, withdrawn at a speed of 20 mm sec^{-1}, and dried in 423 K for 1 minute. This dipping-withdrawal-drying process was repeated in 5 times, and at last the sample was heat-treated in 523 K for 10 minutes. Mg plate was cut in 10 × 50 mm and immersed in 10 wt% nital (nitric acid-ethanol solution) for surface cleaning, and then the same dip-coating process is treated. In order to check the synthesis or growth of coating layer, the weight of sample is measured at the end of every dipping-withdrawal-drying process.

4.2.2 Evaluation of corrosion resistance of silica-coated copper and magnesium

The corrosion behavior of the samples was evaluated by the electrochemical evaluation. The polarization curve was measured in a 3.5 wt% NaCl aqueous solution by a potentiostat/galvanostat (Hokuto Denko Co., Ltd., HA-151) using a Pt electrode (90 mm^2) as a counter electrode and an Ag/AgCl electrode (BAS Inc., RE-1S) as a reference electrode. The reactive area of the sample was adjusted to 61 mm^2 and tested as a working electrode. First, the spontaneous potential was measured for 30 minutes, and the potential was swept to a value of 0.50 V higher than the spontaneous potential at a rate of 1.0 mV sec^{-1}. Similarly, in the same condition, the spontaneous potential was also measured for 30 minutes, and the potential was swept to a value of 0.50 V lower than the spontaneous potential at a rate of 1.0 mV sec^{-1}. Furthermore the salt spray test for 1 week was also attempted.

4.3 Results and Discussions

The thermal stability of APTES dried in 523 K is examined by thermogravimetry (TG) as shown in Figure 4.3. It is assumed that the aminopropyl group of APTES is decomposed at

about 723 K, since the drastic drop of weight at about 723 K is accorded with the molecular weight change of decomposition of the aminopropyl group. Therefore, the modified network structure of APTES is maintained even in the heat-treatment of 523 K.

Figure 4.4 shows the weight change per 1 mm^2 of Cu and Mg substrate with every dipping-withdrawal-drying process. The weight changed largely in the first dipping process, and gradually increased up to third dipping, which indicates a coating layer was deposited from the first dipping to the third dipping process. The final amount of coating layers on both Cu and Mg was about 2.4 μg per 1 mm^2, which indicates coating layers in similar thickness were synthesized on Cu and Mg. However, in the first dipping, the deposition amount on Cu substrate is about twice larger than the amount on Mg substrate, which suggests that the APTES has better adhesion property with Cu.

Figure 4.5 shows the appearance of coated Cu observed by a microscope. The surface of the product is iridescent due to the interference of light by thin film on the metal, and thus, the film formed on the metal is estimated to be submicron scale.

The electrochemical measurement of coated Cu is not available, since the current density of coated Cu is below the detection limit of the equipment (1 nA). In other words, Cu is strongly coated by an insulated layer by the dip coating. Figure 4.6 shows the result of a salt spray test of full-coated and half-coated Cu plate. The corrosion product is observed on the edge of coated area, but the corrosion resistance is distinctly improved by coating.

Figure 4.7(a) shows the Tafel plots of the polarization curve of coated Mg. The tafel plots of raw Mg are drawn in the same graph as a reference. The exchange current density at the corrosion potential (corrosion current density, i_{corr}) of coated Mg is 4×10^{-2} mA cm^{-2}, and it is 5 times lower than the corrosion current density of Mg, which indicates the corrosion

resistant film is formed on the Mg substrate. However, the increase of corrosion resistance is still inadequate, and after the salt spray test, Mg substrate is entirely dissolved and only the squashily damaged coating layer remains as shown in Figure 4.7(b). The silica layer shows the different adhesion property to Cu and Mg, which is due to the different conditions of the surface of these metals. In other words, the oxide layer of Cu is entirely removed by acid, while the surface of Mg is strongly influenced by oxidation even after the acid pickling. For more reliable coating with good adhesion property to Mg substrate, handling Mg in an inert atmosphere or further optimizations of sol-gel solution with a function for removing the oxide layer are considered to be needed.

4.4 Conclusions

In this chapter, we have demonstrated the silica-coating of Cu and Mg for the improvement of corrosion resistance. As the sol-gel solution for silica-coating, trifunctional silane solution of APTES is effective to give flexibility to the film and avoid the cracks. Moreover, APTES shows the good adhesion property to Cu, and Cu is so strongly coated by an insulated layer that the electrochemical measurement is not available. After the 1 week salt spray test, some corrosion products are observed on the edge of samples. The corrosion current density i_{corr} of silica-coated Mg is about 5 times lower than that of raw Mg, but the silica-coating of Mg is not so strong as Cu, and corrosion resistance is not improved in salt spray test. To achieve the firm coating, further optimization of sol-gel solution and handling atmosphere is needed.

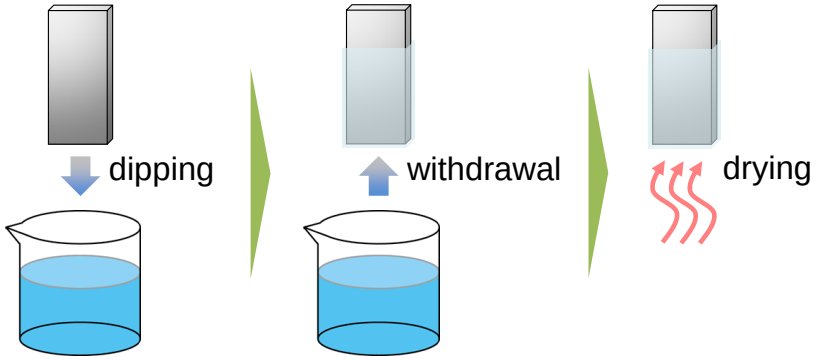

Figure 4.1 Schematic illustration of dip coating procedure.

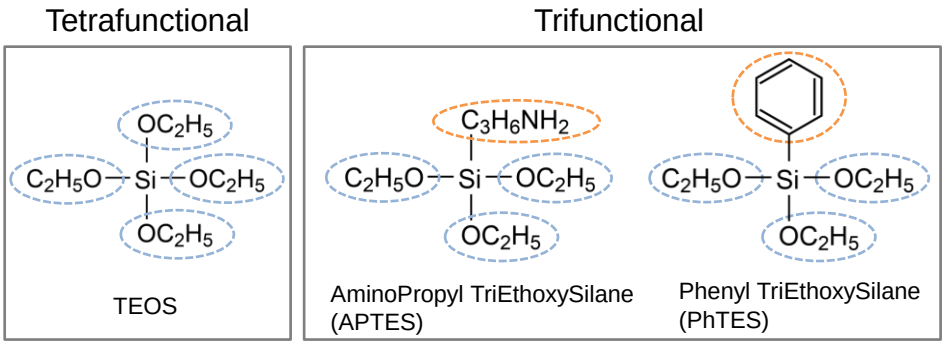

Figure 4.2 Structual formulae of tetrafunctional silane (TEOS) and trifunctional silane (APTES and PhTES).

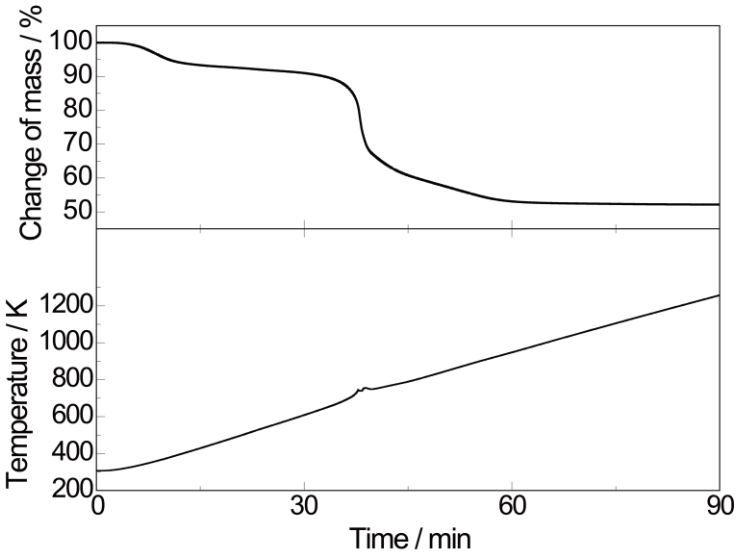

Figure 4.3 Result of thermogravimetric measurement of APTES dried in 523 K.

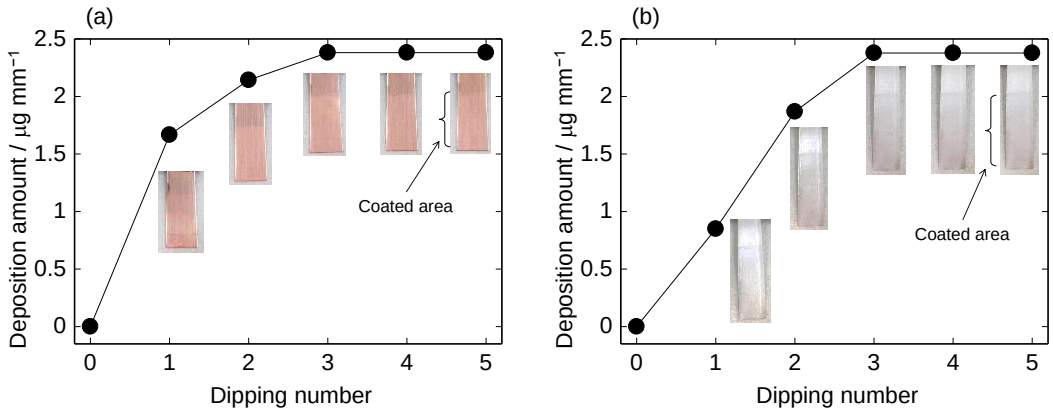

Figure 4.4 Appearances and deposition amounts per 1 mm^2 of (a) Cu substrate and (b) Mg substrate after every dipping-withdrawal-drying process.

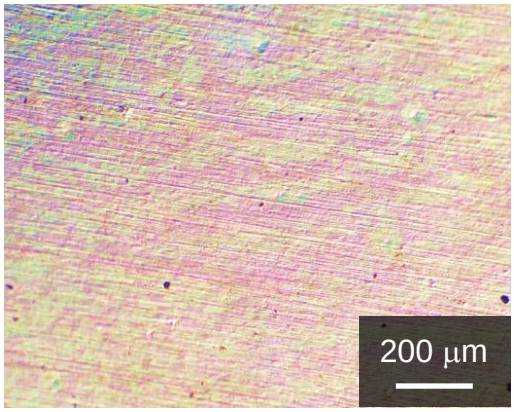

Figure 4.5 Microscopic photograph of silica-coated Cu substrate.

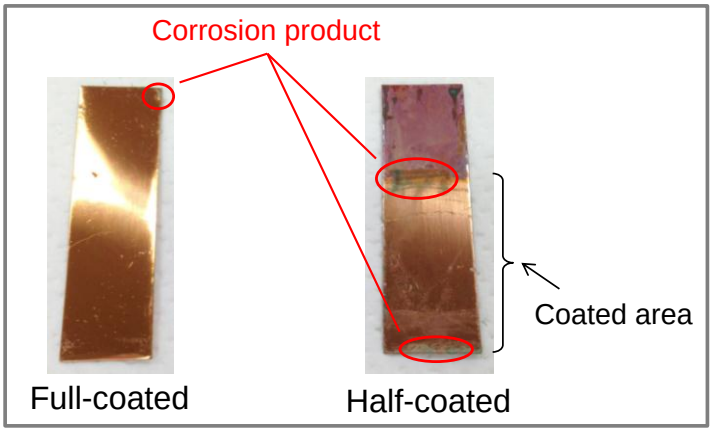

Figure 4.6 Result of 1 week salt spray test of silica-coated Cu.

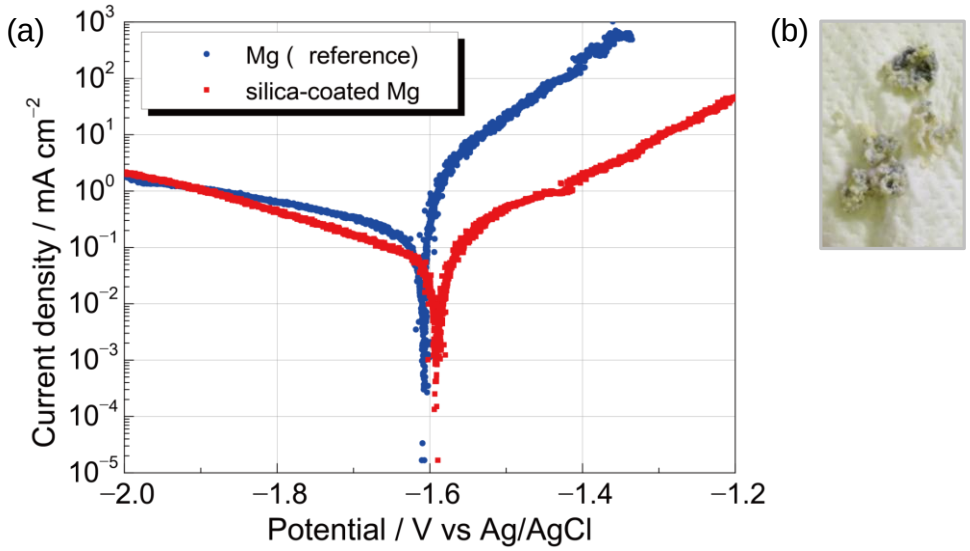

Figure 4.7 (a) Tafel plots of silica-coated Mg and raw Mg, and (b) result of 1 week salt spray test of silica-coated Mg.

References

1. T. L. Barr, *J. Phys. Chem*., **82**, 1801 (1978).
2. B. R. Strohmeier, *Surf. Interface Anal.*, **15**, 51 (1990).
3. N. Sato and K. Kudo, *Electrochim. Acta*, **16**, 447 (1971).
4. S. Yagi, A. Sengoku, K. Kubota and E. Matsubara, *Corros. Sci.*, **57**, 74 (2012).
5. S. Yagi, K. Kuwabara, Y. Fukuta, K. Kubota and E. Matsubara, *Corros. Sci.*, **73**, 188 (2013).
6. C. J. Brinker, G. C. Frye, A. J. Hurd and C. S. Ashley, *Thin Solid Films*, **201**, 97 (1991).
7. Y. Lu, R. Ganguli, C. A. Drewien, M. T. Anderson, C. J. Brinker, W. Gong, Y Guo, H Soyez, B. Dunn, M. H. Huang and J. I. Zink, *Nature*, **389**, 364 (1997).
8. S. Sakka, *Science of Sol-gel Process*, Agne-shofu (1988).
9. B. Mahltig, H. Haufea and H. Böttcher, *J. Mater. Chem*., **15**, 4385 (2005).
10. K. Katagiri, K. Hasegawa, A. Matsuda, M. Tatsumisago and T. Minami, *J. Am. Ceram. Soc.*, **81**, 2501 (1998).
11. X. H. Gu, G. Xue and B.C. Jiang, *Appl. Surf. Sci.*, **115**, 66 (1997).
12. J. P. Gudas and H. P. HACK, *Corrosion*, **35**, 67 (1979).
13. W. Hou and C. Liang, *Corrosion*, **55**, 65 (1999).
14. A. Pardoa, M.C. Merinoa, A.E. Coya, R. Arrabalb, F. Viejob and E. Matykina, *Corros. Sci.*, **50**, 823 (2008).
15. L. Li and A. A. Sagüés, *Corrosion*, **57**, 19 (2001).
16. G. Song, A. L. Bowles and D. H. StJohn, *Mater. Sci. Eng*., **366**, 74 (2004).
17. H. Hoche, H. Scheerer, D. Probst, E. Broszeit and C. Berger, *Surf. Coat. Tech*., **174**, 1018 (2003).
18. C. H. Pyun and S. M. Park, *J. Electrochem. Soc*., **133**, 2024 (1986).

19. I. Milošev and M. Metikoš‐Hukovic, *J. Electrochem. Soc*., **138**, 61 (1990).

20. A.V. Benedeti, P.T.A. Sumodjo, K. Nobe, P.L. Cabot and W.G. Proud, *Electrochim. Acta*, **40**, 2657 (1995).

21. E. McCafferty, *Corros. Sci.*, **47**, 3202 (2005).

22. Z. Shi, M. Liu and A. Atrens, *Corros. Sci.*, **52**, 579 (2010).

Chapter 5

Summary

In this study, the silica-coating techniques are developed in various fields of stabilization for metals. The sol-gel process was an appropriate approach for low-temperature synthesis of silica, and thus, the metals which are easily oxidized were successfully coated by silica-shells. Moreover, we have suggested not only the method of silica-coating, but also the quantitative evaluation of dissolution and deposition behaviors based on QCM and electrochemical measurements, and we have also demonstrated the improvement of corrosion resistance of metals in some applications. The brief summary for each chapter is described as follows.

Chapter 2

The Cu@SiO_2 (silica-coated Cu) nanoparticles were successfully synthesized by the electroless deposition of Cu and the sol-gel method of TEOS. In this synthesis procedure, the formation rate of silica-shells should be faster than the dissolution of Cu, and thus, the evaluation of dissolution behavior of Cu and deposition speed of silica is important. In the previous reports, we have demonstrated that the "deposition behavior" of metallic nanoparticles is effectively estimated by the QCM measurement combined with the electrochemical evaluation, but in this work, we also suggested that the measurement of QCM and mixed potential is a powerful tool for verifying the "dissolving behavior" of Cu. This accurate optimization method which we reported in this study is applicable to other metals of fabricating the core-shell structures, and the quantitative evaluations of dissolution of Cu-core and formation of silica-shells enabled us to synthesize the silica-coated Cu nanoparticles.

Moreover, the tight and strong silica-shells were formed by an appropriate heat-treatment.

Chapter 3

In this chapter, the red color glaze was achieved by using the SiO_2-coated Cu nanoparticles. In this work, the red color of *shinsha* glaze was set as the target color, and we demonstrated the nearest red color by firing the mixture of 1.0 g *raku*-frit, 0.04 g SiO_2-coated Cu nanoparticles and 0.003 g Si powder. Also, we found that the key of characteristic deep red color of *shinsha* glaze is blue glass layer formed on the top of relatively bright red layer, and thus, the appropriate blue glass layer may enable the color of fired glaze using SiO_2-coated Cu nanoparticles to conform the color of *shinsha* glaze. In terms of the SiO_2-coated Cu nanoparticles, red color was achieved even without Si powder, which indicates the Cu-cores were sufficiently protected by the SiO_2-shells during the firing of glaze (1073 K).

Chapter 4

As the further application of the silica-coating technique, the fabrication of transparent corrosion resistant films for bulk metals was attempted. Specifically the dip coating method of aminopropyl triethoxysilane (APTES) was developed in this chapter. As the sol-gel solution for silica-coating, we found that the trifunctional alkoxysilane solution of APTES is effective to give flexibility to the film and avoid the cracks. Moreover, the fabricated coating layer showed good adhesion property to Cu, and strong corrosion resistant film was formed. Mg was also coated by the dip coating method, and the corrosion resistant property of silica-coated Mg evaluated by an electrochemical measurement was better than that of raw

Mg. However, silica-coated Mg was dissolved by a salt spray test, which indicates the silica-coating layer formed in this dip coating procedure had insufficient performance for a corrosion resistant film.

List of Publications

Paper

"Development of Red Color Glaze Using Copper by Oxidation Firing"

Hajime Taguchi, Shozo Hashida, Tadanori Yokoyama, Shohei Shiomi, Shunsuke Yagi, and Eiichiro Matsubara,

Research Report of Kyoto Municipal Institute of Industrial Technology and Culture, (2012)

"Synthesis of Silica-coated Copper Nanoparticles and its Application to Red Color Glaze"

Shohei Shiomi, Eiichiro Matsubara, Hajime Taguchi, Shozo Hashida, and Tadanori Yokoyama,

Adv. mater. res., in press.

"Synthesis of Silica-coated Copper Nanoparticles Based on the Developed QCM Evaluation"

Shohei Shiomi, Makoto Kawamori, Shunsuke Yagi, and Eiichiro Matsubara,

(in preparation)

Patent

"Composite Nanoparticle and Method for Producing the Same, Glaze, and Method for Producing Metal Nanoparticle" (P130008537)

Eiichiro Matsubara, Shohei Shiomi, Hajime Taguchi, Shozo Hashida, and Tadanori Yokoyama,

July 21, 2011 (Filing), February 4, 2013 (Publication)

Oral Presentation

"Synthesis and Application of Silica-coated Cu nanoparticles"

Shohei Shiomi, and Eiichiro Matsubara,

Joint Symposium on the Materials Science and Engineering for the 21st Century 2011, Nanyang Tech. Univ., Singapore, June 19 to 23, 2011

"Synthesis of Silica-coated Cu nanoparticles"

Shohei Shiomi, and Eiichiro Matsubara,

The 221st Meeting of the Electrochemical Society, Seattle, Washington, May 6 to 10, 2012

"Synthesis of Silica-coated Cu nanoparticles and its Applications"

Shohei Shiomi, Eiichiro Matsubara, Hajime Taguchi, Shozo Hashida, and Tadanori Yokoyama,

The 1st International Conference on the Science and Engineering of Materials, Kuala Lumpur, Malaysia, November 13 to 14, 2013

Poster Presentation

"Silica-coating of Copper Nanoparticles and its Application to Red Color Glaze"

Shohei Shiomi, Eiichiro Matsubara, Hajime Taguchi, Shozo Hashida, and Tadanori Yokoyama,

The 10th Meeting of the Japanese Sol-Gel Society, Keio Univ., Kanagawa, July 26 to 27, 2012

(Best Poster Presentation Award)

Acknowledgements

I would like to express my deep gratitude to Professor Eiichiro Matsubara for offering a number of invaluable advices and discussions at any time. I would also like to thank Associate Professor Tetsu Ichitsubo for his discerning suggestions and discussions. Also, I am grateful to Dr. Shunsuke Yagi for his considerate coaching from my undergraduate research. I would like to express my thanks to Dr. Masatsugu Oishi, Professor Noboru Yamada, Dr. Satoshi Toyoda and Mr. Kenji Kazumi for their helpful support and assistance in experimental works.

I would like to express my acknowledgements to Ms. Mari Otogawa, Ms. Tomoe Weedall and Ms. Asako Hasegawa for a wide variety of clerical supports. I also would like to express my special thanks to Mr. Hidetaka Nakanishi, Dr. Yu-ki Taninouchi, Dr. Mary Donnabelle Lirio Balela, Dr. Makoto Kawamori, Mr. Tomoya Kawaguchi, and of course all other members of Professor Matsubara's laboratory for numerous assistances and delightful discussions.

I would like to express my gratitude to Mr. Hajime Taguchi and all other members of Kyoto Municipal Institute of Industrial Technology and Culture for kind assistances and supports.

Finally, I am especially grateful to my father, Masanari Shiomi, and my deceased mother, Akiyo Shiomi, and my grandmother, Sumiko Hosomi, for their supports and backups.

I had a precious time and valuable experiences throughout my research life in Kyoto University with all my dear staffs, students, associates, and family.

Shohei Shiomi